RESPONSE OF A PILE RESTRAINED FLOATING BREAKWATER

by

BRENDA MANUEL

B.E.Sc, University of Western Ontario 1995

A THESIS SUBMITTED IN PARTIAL FULFILLMENT OF
THE REQUIREMENTS FOR THE DEGREE OF
MASTER OF APPLIED SCIENCE

in

THE FACULTY OF GRADUATE STUDIES
DEPARTMENT OF CIVIL ENGINEERING

We accept this thesis as conforming
to the required standard

THE UNIVERSITY OF BRITISH COLUMBIA

August, 1997

Department of Civil Engineering
The University of British Columbia
2324 Main Mall
Vancouver, B.C., V6T 1Z4
Canada

22 Aug. 1997.

Abstract

Experimental work has been performed to assess the behaviour of a caisson-type floating breakwater restrained by adjacent vertical piles. A series of two-dimensional simulations were executed evaluating the effectiveness of the breakwater as it was subjected to various incident wave trains. The transmission coefficient was of primary interest, although the reflection coefficient, energy dissipation coefficient, and heave response amplitude operator were also evaluated from the experimental results. Two numerical models were used to estimate the reflection coefficient from the experimental data; the two-probe method and the least squares method. Numerical analysis was executed using the Hydrodynamic Analysis of a Floating Breakwater software (HAFB), which is a model based on linear wave diffraction theory to predict wave loads and motions of a floating breakwater in oblique seas. This model was used to numerically predict the transmission and reflection coefficients and the heave response amplitude operator. The results of the numerical model show reasonable agreement with the experimental results.

TABLE OF CONTENTS

List of Tables

List of Figures

Nomenclature

A_n	measured wave amplitude at the nth probe
A_n'	theoretical wave amplitude at the nth probe
a	characteristic dimension of breakwater(half beam used)
a_i	incident wave amplitude
a_r	reflected wave amplitude
B	breakwater beam
C_j	exciting force coefficients
C_w	wave drift force coefficient
c_{ij}	hydrostatic stiffness matrix
d	still water depth
f	wave frequency
g	gravitational constant
H	wave height
H_i	incident wave height
H_r	reflected wave height
H_t	transmitted wave height
k	wave number
K_e	energy dissipation coefficient
K_r	reflection coefficient
K_t	transmission coefficient

L	wave length
m	mass per unit length of the breakwater
m_{ij}	mass matrix
r_y	radius of gyration about center of gravity
t	time
T	wave period
v_{ij}	viscous damping matrix (numerical analysis)
W	breakwater width
x	horizontal distance orthogonal to reflecting boundary
x_n	x coordinate of nth probe
y	horizontal distance orthogonal to x
Z_j	response amplitude operator
z_b	z coordinate of center of buoyancy
z_g	z coordinate of center of gravity
β	phase angle of reflected wave train
Δ_n	dimensionless probe spacing, $k\lambda_n$
δ_n	measured phase at nth probe relative to phase at first probe
η	free surface elevation
λ_n	distance between nth and first probes
ρ	water density
ϕ_n	theoretical wave phase at nth probe

χ	$2kx_1 - \beta$
ω	wave angular frequency
ξ_i	amplitude of breakwater heave motion

Acknowledgments

The author would like to express her gratitude and appreciation to Dr. Michael Isaacson for his support and guidance throughout the writing of this thesis. His committed involvement and dedicated interest in the present work was much appreciated throughout the process. Support through a research assistantship is also greatly appreciated from the University of British Columbia, Department of Civil Engineering.

Many thanks are also extended to colleagues in the Ocean and Coastal Engineering program at UBC, particularly Nathalie Garceau, Sundaralingam Premasiri and Shankar Bhat, for their willing assistance and direction in the experimental stages of this thesis.

1.0 INTRODUCTION

1.1 Floating Breakwaters in Coastal Engineering

The Pacific coast of Canada contains large areas of protected waters with abundant recreational boating opportunities. These areas also support many commercial fishermen using small boats in their fishing operations. As a result, there is a large demand for sheltered moorage for vessels. In many cases marinas, fishing harbours, and aquaculture operations are partially protected from wave action by natural topographic features such as islands, shoals and spits. However, more exposed regions are being considered for marinas and small craft facilities because of the increased demand, and consequently many sites require further protection.

Traditionally, rubble-mound breakwaters have been constructed for marina and harbour protection against wave attack. Such bottom-founded breakwaters involve an increase in cost with the water depth, thus the expense can become prohibitive in deeper water. Furthermore, rubble-mound breakwaters reduce water circulation within protected areas, leading to an increased concentration of pollutants within the protected area. They may also give rise to sedimentation problems.

In contrast, a floating breakwater does not interfere with the interchange of water, sediment transport or marine life migration and the cost is relatively independent of depth. A floating breakwater can also be placed in areas where the sea bottom condition is unsuitable for the construction of a traditional rubble-mound breakwater. This solution introduces a more attractive alternative which avoids many of the problems and restrictions outlined above, while satisfying moorage demands. Sites where floating breakwaters may be preferable to traditional bottom-founded structures are characterized by a moderate wave climate sheltered from long period waves by surrounding land masses, large tidal fluctuations and/or a steeply sloping seabed – conditions which would make a bottom-founded structure very expensive. Additionally, because floating breakwaters are conveniently portable, they can be advantageous for temporary or seasonal protection.

The primary limitations to most floating breakwater designs include the loss of their wave attenuation characteristics as the length of the incident waves become substantially large, and the failure of mooring systems or connections between units. Since the longest and largest waves at a given site generally coincide with the most severe storms, the effectiveness of the breakwater can potentially be lost when it is most critically needed. As a result, the application of floating breakwater systems is generally confined to relatively sheltered and fetch-limited bodies of water where incident wavelengths have a fairly well defined upper bound.

1.2 Floating Breakwater Designs in Use

Despite limitations, careful selection of design criteria can produce a breakwater which satisfies wave attenuation requirements and provides shore or harbour protection where traditional bottom-founded designs would be impractical to construct. Due to their economy, flexibility and relative depth independence, floating breakwaters often present an attractive solution to the problem of sheltering small craft harbours from attack by wind waves and boat swell. They must however, be sited, designed and utilized with care.

A diverse variety of floating breakwaters have been developed and used, ranging from very simplistic schemes to complex and expensive designs. Presently, there are hundreds of floating breakwaters in use throughout the world. Floating breakwaters have been used in China as water diversion channels in reservoirs along with extensive wave protection systems. They have also been implemented for aquaculture use and have been applied in the field for protection in the operation area of dredgers (Yao, 1993). British Columbia is equipped with numerous floating breakwaters, including a unique and innovative solution comprised of five non-operational cargo ships lined up on end.

Breakwater designs can be classified in a variety of ways. One classification facilitates the wave reducing mechanism where two basic mechanisms are used, either in combination or alone, to attenuate wave heights within the protected area. The first mechanism, wave reflection, occurs where a portion of the incident wave energy is reflected from the face of the breakwater as if it were a fixed obstacle. The second is energy dissipation, where turbulence induced by either wave breaking or wave-structure interaction causes dissipation of incident wave energy.

The diversity of breakwater types can be classified into two broad categories according to the above mechanisms. Pontoon breakwaters rely primarily on these two mechanisms, whereas dissipative breakwaters rely on wave-induced turbulence in order to dissipate wave energy. From the point of view of wave dissipation mechanisms, floating breakwaters can be classified into the following three categories:

a) Reflection-type structures - these reflect most of the incident wave energy to the offshore side. Typical examples include the caisson-type and pontoon-type breakwaters.

b) Reflection and wave breaking-type structures - these encourage wave breaking and thereby attenuate both the reflected and transmitted waves. The barrier-type and pontoon-barrier-type breakwaters are typical examples.

c) Friction-type structures - incident wave energy is attenuated by friction and the transmitted wave decays according to the magnitude of energy loss through the breakwater. The mattress-type and sheet-type floating breakwaters are examples of this kind of structure.

Three of the most common breakwaters found in British Columbia include concrete caissons, log bundles and the A-frame type breakwater. In the case of concrete caissons, the large mass of the section provides a relatively stable vertical barrier able to resist the motions of waves by virtue of its inertia. Most caisson designs are essentially similar in construction, consisting of a reinforced concrete box divided into internal sections by means of integral partitions, much like an inverted ice-cube tray. The interstitial spaces are sometimes left empty allowing the trapped air to provide buoyancy, however, the space is more commonly filled with closed-cell plastic foam to provide positive buoyancy in the event of a structural failure in the caisson wall. Most designs have a smooth, flat deck surface, making them amenable to ancillary uses such as pedestrian walkways and boat moorage. Floating log bundles are used extensively throughout British Columbia, although in their simplest application - a mere boom of single logs - they are not effective against any but the shortest period waves. Lastly, an A-frame breakwater normally consists of steel pontoons and a timber centerboard extending vertically downward from the sea surface. While providing significant roll-stability, it is less resistant to heave due to the small mass per unit length.

Several breakwater structures have been designed and tested with a range of different varibles. For example, a number of distinct breakwater systems were tested by Aoki, Kim and Sawaragi, 1994, in which twelve different breakwater configurations were considered. They found no difference between the results for the cases using single float and double floats. The use of side skirts was also seen to be effective in reducing wave transmission by increasing the wave reflection. The most effective breakwater model was the double pontoon with a side skirt. In their experiments, steel piles and movable mooring attachments were used to avoid both the jerky movement of the floating unit and the impulsive forces on the piles. Results indicated that large initial constrictive forces did not effectively reduce the wave transmission, and further suggested that it may be possible to reduce the movement of the floating breakwater without a decline in the breakwater performance.

Another interesting concept in breakwater design is a dynamic breakwater, which incorporates a set of buoys anchored at the sea bottom and floating under the water surface. In this instance, each buoy has a resonant frequency near that of the anticipated predominant waves for a given location. This would cause the buoys to pendulate back and forth in the incoming waves out of phase with the wave orbital motions. The effect of this wave-excited buoy motion would be to transform wave energy into water turbulence and then heat in the wake of the buoy (Agerton, 1976).

1.3 Performance of Existing Floating Breakwaters

To assess the performance of a floating breakwater, the single parameter which is most widely used is the transmission coefficient, K_t, defined as the ratio of transmitted to incident wave height. In conducting field experiments, or in developing theoretical models, the variables affecting performance which need to be measured include:

- Transmitted waves
- Reflected waves
- Energy dissipation
- Motions of the breakwater
- Forces on the mooring lines

Presently, most floating breakwater applications are for short-period wind wave or boat wake protection at semi-sheltered sites in estuaries, reservoirs, lakes and rivers. According to McCartney (1985), the limiting design wave, for single box or pontoon type breakwaters is 4 feet high and a 4 second period. Most floating breakwaters are constructed using discrete modules connected together, whereas other designs have incorporated a continuous structure. The caisson-type breakwaters were found to have better transmission characteristics in which the catamaran configuration has performed best (McCartney, 1985).

Pile restrained breakwaters are limited to fairly shallow sites (about 9 m depth) and require suitable bottom material to allow adequate pile penetration and sufficient lateral strength. Stake piles can be steel H beams or timber. Generally, they are driven below the mud line to develop the greatest strength and prevent destruction of wood piles by marine borers. Stake piles are suitable for fairly firm foundations and water depth less than 15.2 m (McCartney, 1985).

1.4 Scope of Project

The purpose of this work is to evaluate the performance of a typical rectangular floating breakwater confined by vertical piles. Floating breakwaters restrained by piles allow the breakwater to rise and fall with both the tide and waves, while being laterally restrained. This study considers a pile restrained floating breakwater as a semi-fixed floating structure in which the sway, surge, yaw, roll and pitch modes are strongly constricted, but the structure is essentially free to move in the heave direction. The behaviours of such semi-constricted floating breakwaters are first investigated by experiments which examine the characteristics of wave transmission, wave reflection, energy dissipation and body motion. Four sets of experiments were performed with variations in wave steepness, wave period and restraint system (gap between the piles and the breakwater; including freely floating and fixed cases). Secondly, a numerical model is used to investigate the above characteristics on the basis of the linear potential theory. Results from both the experimental and numerical analyses are compared and discussed.

2.0 THEORETICAL BACKGROUND

2.1 Regular Uni-Directional Waves

The primary purpose of a breakwater is to reduce wave heights generated by either wind or a ship's wake. This is achieved as an incident wave approaches the breakwater and converts the wave energy via reflection, absorption, and dissipation through turbulence created by inducing breaking and by friction. The general case of normal reflection of regular waves assumes the free surface elevation to correspond to the superposition of sinusoidal incident and reflected wave trains. For convenience, the origin of the horizontal coordinate x may be defined as the intersection of the reflecting structure with the still water level. The water surface elevation η in front of the barrier may be expressed as:

$$\eta = a_i \cos(kx-\omega t) + a_r \cos(-kx-\omega t+\beta) \tag{2.1}$$

where a_i and a_r are the amplitudes of the incident and reflected wave trains, respectively, β is the phase angle that describes the phase of the reflected waves as the phase difference between the incident and reflected wave trains at $x = 0$ or $t = 0$, k and ω are the wave number and wave angular frequency respectively, related by the linear dispersion relation:

$$\omega^2 = gk \tanh(kd) \tag{2.2}$$

where d is the still water depth, g is the gravitational constant and k is the wave number. The positive performance of a breakwater is generally measured by a transmission coefficient, K_t, defined as:

$$K_t = \frac{H_t}{H_i} \tag{2.3}$$

where H_t is the transmitted wave height and H_i is the incident wave height. Similarily, a reflection coefficient is defined as:

$$K_r = \frac{H_r}{H_i} \tag{2.4}$$

where H_r is the reflected wave height.

The energy dissipation coefficient K_e is defined as the proportion of incident wave energy flux that is dissipated by the barrier. A balance of energy flux requires that the energy flux of the incident wave train is equal to the energy flux of the transmitted and reflected wave trains together with the energy flux that is dissipated. Since energy flux is proportional to wave height squared, an energy balance gives the following relationship:

$$K_r^2 + K_t^2 + K_e = 1 \tag{2.5}$$

2.2 Dimensional Analysis

Controlled variables in model tests can be varied in a meaningful way through the application of a dimensional analysis. This is carried out for a rigid breakwater extending to a depth h below the still water level and subjected to a uni-directional, regular, non-breaking wave train propagating normally to the breakwater (Fig. 1). There are a number of dependent variables which are indicative of barrier performance and are used in design. These include the reflection wave height, the transmitted wave height, the run-up and the wave loads. Dimensional analysis applied to the reflection coefficient, K_r, and transmission coefficient, K_t, may be expressed in the following form (note that the influence of viscosity and therefore Reynolds number has been omitted):

$$K_r = f_1\left(ka, \frac{H}{L}, kd\right) \tag{2.6}$$

$$K_t = f_2\left(ka, \frac{H}{L}, kd\right) \tag{2.7}$$

where H is the incident wave height, L is the wave length, d is the water depth, and a is a characteristic dimension of the breakwater (a = B/2 was used in this study).

2.3 Numerical Model

The computer model HAFB (Hydrodynamic Analysis of a Floating Breakwater) has been used to predict breakwater motions, and is based on work of Isaacson and Nwogu (1987). The program uses linearized potential theory to predict the wave loads and motions of a floating breakwater by computing the exciting forces and hydrodynamic coefficients due to the interaction of a regular wave train with an infinitely long, semi-immersed floating breakwater. The boundary element method is applied to formulate the problem in terms of a distribution of sources around the breakwater, the free surface and upward and downward radiation boundaries. The method involves an unknown scatter potential ϕ_s which is represented by a distribution of two-dimensional "point sources" over a surface S, containing the fluid region up to a finite distance away from the structure. The application of the appropriate boundary conditions gives rise to an integral equation for the unknown source strengths. A discretization of the surface S into a finite number of segments reduces the integral equation to a matrix equation which can be solved for the unknown source strengths. Once the source strengths are known, the velocity potential, and hence the transmission coefficient and other hydrodynamic coefficients can be evaluated.

The program HAFB allows the breakwater cross-section to be specified as rectangular, circular or to be of arbitrary shape. Breakwater section properties such as the centre of gravity, the radius of gyration, the centre of buoyancy and the viscous damping coefficients for sway, heave, and roll also need to be specified. The exciting force, added mass, damping coefficient and response amplitude operator are calculated for sway, heave and roll corresponding to a specified incident wave frequency and direction. In addition the reflection and transmission coefficients are also provided. In the present context, calculations may be carried out for a number of different conditions including the fixed, freely floating and pile restrained breakwater.

The equations of motion are solved to predict the complex amplitudes of motion for each wave frequency and direction. The output lists the mass, stiffness and viscous damping matrices together with the natural period of oscillation, the response amplitude operators and the wave drift force coefficient, reflection coefficient, transmission coefficient and energy dissipation coefficient. For the purpose of this study, hydrodynamic coefficients and heave values are the main concern. The heave RAO (response amplitude operator) is defined as follows:

$$\mathrm{RAO}_i = \frac{|a\xi_i|}{H/2} \tag{2.8}$$

where ξ is the amplitude of the heave motion.

3.0 EXPERIMENTAL INVESTIGATION

3.1 Introduction

The full-scale performance of a breakwater in the field is generally difficult to predict without great expense and effort. Scale models have become a much more economical and convenient way of analyzing certain behaviours when numerical models are not available or have not yet been proven as reliable predictors. Particular pile restrained model tests have been performed in the wave flume in the Hydraulics Laboratory at the University of British Columbia, Canada. The following section describes the methods used in the experimental set-up for wave generation and data acquisition, and examines the data analysis and results of hydrodynamic coefficients and floating body motions.

3.2 Model Breakwater

The proposed breakwater design entails a rectangular caisson structure restrained by four vertical piles at each corner, as shown in Figs. 2 and 3. Under an ideal friction-free condition, the pile restrained breakwater permits free movement in heave and inhibits motion in all other directions. In this particular study, the piles were mounted vertically on a steel plate at the bottom of the wave flume and secured with a second steel plate connecting the tops of each pile. The model had dimensions as follows: a length of 0.53 m, a beam of 0.3 m, and a height of 0.2 m, with the four restraining piles placed 0.1 m in from the wall at each corner (Fig. 3). Effects due to friction between the breakwater and the flume wall were decreased with the use of rollers. The material used for the main components of the model was Plexiglas because of its low density. Weights were added within the model so as to maintain the draft at a constant value of 0.1 m.

3.3 Experimental Facilities and Measurement Equipment

A view of the Hydraulics Laboratory wave flume is shown in Fig. 4 and as previously stated, Fig. 2 shows a sketch of the experiment set-up. The flume measures 0.62 m in width, 0.9 m in height and 20 m in length from the paddle to the holding tank. A 7 m long artificial beach consisting of plywood set at a 1:15 slope covered with artificial hair matting extended from the downwave end of the tank. The beach, combined with the holding tank, effectively absorbs and dissipates wave energy preventing significant wave reflection. The flume was operated with a water depth of 0.5 m, and wave periods ranging from 0.8 to 2.0 sec. The wave height was altered by adjusting the stroke of the wave paddle, but kept small enough so that overtopping was minimized. The flume is equipped with a computer controlled wave generator capable of producing both regular and random waves, although only regular waves were used in this study. The model breakwater was placed 7.6 m down from the wave paddle, see Fig. 5.

Wave transmission and reflection coefficients were estimated by using the simultaneous records of water surface elevation measured by sets of wave gauges on both sides of the breakwater. A three probe array was used to measure reflection coefficients where three probes were placed between the model and the wave generator, at distances of 1.0 m, 1.2 m, and 1.45 m from the centre of the breakwater. Analysis of the transmission coefficients was achieved using two probes placed between the model and the holding tank at 1.0 m and 1.2 m from the breakwater centerline. The selection of the probe locations took into consideration evanescent wave modes, the wave paddle location, and the various reflection analysis methods to be considered.

Not only are the transmitted and reflected waves of importance, but so too are the breakwater motions, particularly the heave motions which are relevant in the present study, see Fig. 6. The corresponding vertical displacements were measured by a Super VHS video camera with respect to a grid placed on the side of the flume. This gave an accurate estimation of the heave motion with an estimated error of +/- 0.5cm.

The data acquisition system captures analog signals produced by wave probes, converts them to digital information, and transmits them to a computer system. The computer used to control the experiment was a Digital Equipment Corporation (DEC) VAX station 3200. The GEDAP (Generalized Experiment control, Data acquisition and Analysis Package) library of software (Miles, 1989) and associated RTC (Real Time Control) (Pelletier, 1989) programs developed by the National Research Council of Canada, were used to control the wave generation and data acquisition processes. This general purpose software package was used extensively during all stages of the experimental investigation. GEDAP is a fully integrated, modular system linked together by a common data file structure, which maintains a standard data file format such that it can process data generated by any other GEDAP program. The GEDAP program also includes a set of data analyzing programs which enables the processing of projects involving various parameters and constraints with little or no project specific programming. An attractive feature is a fully integrated interactive graphics capability, enabling an easy examination of results at any stage of the data analysis process. It also includes an extensive collection of utility packages, which consists of a data manipulation routine, a frequency domain analysis routine, as well as statistical and time-domain analysis routines. In particular, the program RTC_SIG generates the control signal necessary to drive the wave generator, and the routing RTC_DAS reads the data acquisition unit channels and stores the information in GEDAP binary format compatible with other GEDAP utility programs.

RWREP2 program is used to compute the wave machine control signal for a regular wave train corresponding to a wave height and period specified by the user. The control signal file produced by the program RWREP2 is sent to the wave machine controller through a D/A output channel by using the real-time control program RTC.

The Real Time Control (RTC) software package was used throughout all stages of the experimental procedure. RTC consists of a main hardware execution program and a command entry program that allows the user complete control over data acquisition, control loops and signal generation.

Wave generation was attained by first loading the control signal file into the RTC buffer file, then enabling the buffer to start the wave machine. When the enable command was given, the output signal was gradually ramped up from zero amplitude to full amplitude over a period of 10 seconds. This automatic ramping was carried out in order to protect the wave machine from being subjected to sudden transients in its control signal.

This system allows sampling of the wave probe, where the RTC program was used to measure the wave train produced by the wave machine. Wave elevations were measured using capacitance-type wave probes, measured at a rate of 50 samples per second for a duration of 14 seconds. In order to analyze the wave train it was necessary to demultiplex the data through the PDMULT2 program. Here, the Primary Data File (.PDF) produced by the GEDAP analysis was used to demultiplex the data into five files representing the wave data at each probe. These individual GEDAP compatible data files may then be analyzed by existing GEDAP programs.

3.4 Experimental Program and Procedures

Thirty-nine model tests were performed. It was expected that the wave parameters that would have the greatest influence on the hydrodynamic coefficients would be the wave length L, the wave height H, and the gap spacing G, between the piles and the breakwater. The water depth was held constant at a value of d = 0.5 m for all tests, while the wave period, wave height, and the gap spacing were varied. The first set of tests were carried out using regular waves with wave periods ranging from 0.8 to 2.0 s (measured at 0.8, 1.2, 1.4, 1.6, 1.8, 2.0 s) and H/L varying from 0.02 to 0.08 (measured at 0.02, 0.05, 0.08). The second set of simulations involved variations in the gap (G) between the breakwater and the bottom-founded piles; see Fig. 3 for the definition of gap spacing, G. Tests were run with the total gap, G set at 0, 2, 4 and 8 cm, keeping the steepness (H/L) constant with a varying period. Throughout the experiments, wave heights were kept small in order to minimize wave overtopping.

From the wave probe and video records, the following parameters were obtained for each test:

H	incident wave height
H_r	reflected wave height
H_t	transmitted wave height
ξ	heave response amplitude operator (RAO)
K_r	reflection coefficient (H_r/H_i)
K_t	transmission coefficient (H_t/H_i)
K_e	energy dissipation coefficient

3.5 Data Analysis

3.5.1 Regular Wave Reflection Analysis

There are several methods described in literature for analyzing uni-directional wave reflection. Isaacson (1991) describes and compares three such methods, and concludes that the least squares and two probe methods are generally the most reliable and acceptable. Both methods have been considered in the present analysis and are summarized below.

The free surface elevation, η is assumed to correspond to the superposition of sinusoidal incident and reflected wave trains, where the origin of the horizontal coordinate x is defined at the centre of the breakwater. Time t is taken to be zero when an incident wave crest crosses x = 0, so that the free surface elevation η may be expressed as:

$$\eta = a_i \cos(kx - \omega t) + a_r \cos(-kx - \omega t + \beta) \tag{3.1}$$

where a_i and a_r are the amplitudes of the incident and reflected wave trains respectively, and the phase angle, β, accounts for the phase difference between the incident and reflected wave trains at x = 0 or t = 0. The wave number and wave angular frequency, k and ω respectively, are related by the linear dispersion relation:

$$\omega^2 = gk \tanh(kd) \tag{3.2}$$

where d is the still water depth, and g is the gravitational constant. The incident wave height (H) and reflection coefficient (K_r) are given in terms of a_i and a_r as:

$$H = 2\, a_i \tag{3.3}$$

$$K_r = a_r / a_i \tag{3.4}$$

Equation 3.1 is to be applied at a series of probe locations x_n, n = 1, 2, ... that may be written in terms of the location of the first probe x_1 and the intervals between probes:

$$x_n = x_1 + \lambda_n \tag{3.5}$$

where the distance between the nth probe and the first probe is $\lambda_n (n \geq 2)$ and $\lambda_1 = 0$. A dimensionless form of this expression can be written as follows:

$$kx_n = kx_1 + \Delta_n \tag{3.6}$$

where $\Delta_n = k\, \lambda_n$ is the dimensionless distance between the nth probe and the first probe, and $\Delta_1 = 0$. Equation 3.1 applied at each probe location may thus be written as:

$$\eta_n = a_i \cos(kx_1 + \Delta_n - \omega t) + a_r \cos(kx_1 + \Delta_n + \omega t - \beta) \tag{3.7}$$

The free surface elevation at the n^{th} probe given by (3.7) is an assumed form which can also be expressed in terms of an amplitude A_n and phase ϕ_n. The actual measurements at the probe locations will provide corresponding amplitudes and relative phases, such that the measured elevation at the n^{th} probe may be written as:

$$\eta_n^{(m)} = A_n \cos(\omega t - \phi_n) \tag{3.8}$$

$$= A_n \cos(\omega t - \phi_1 - \delta_n) \tag{3.9}$$

where A_n is the measured amplitude of the n^{th} probe, ϕ_1 is the absolute phase of the first probe which does not need to be measured, and δ_n is the measured phase of the n^{th} wave record relative to the first, so that $\delta_n = \phi_n - \phi_1$.

Least Squares Method

In the least squares method, three probes are used so that A_n, δ_n and Δ_n (n = 1, 2, 3) are measured. Isaacson (1991) provides the solution for H, K_r, and β in terms of these as follows:

$$a_i = |X_i| \tag{3.10}$$

$$a_r = |X_r| \tag{3.11}$$

$$\chi = \mathrm{Arg}(X_i) - \mathrm{Arg}(X_r) \tag{3.12}$$

where

$$X_i = \frac{s_2 s_3 - 3 s_4}{s_5} \tag{3.13}$$

$$X_r = \frac{s_1 s_3 - 3 s_3}{s_5} \tag{3.14}$$

and

$$s_1 = \sum_{n=1}^{3} \exp(i 2 \Delta_n) \tag{3.15}$$

$$s_2 = \sum_{n=1}^{3} \exp(-i2\Delta_n) \tag{3.16}$$

$$s_3 = \sum_{n=1}^{3} A_n \exp[i(\delta_n + \Delta_n)] \tag{3.17}$$

$$s_4 = \sum_{n=1}^{3} A_n \exp[i(\delta_n - \Delta_n)] \tag{3.18}$$

$$s_5 = s_1 s_2 - 9 \tag{3.19}$$

H and K_r are then obtained from a_i and a_r through (3.3) and (3.4) and β may be obtained from the definition of χ, using a measurement of x_1:

$$\beta = 2kx_1 - \chi \pm 2\pi m \tag{3.20}$$

where m = any integer, usually chosen such that $0 \leq \beta < 2\pi$.

The expressions for s_n may be written in alternative forms if required (Mansard and Funke, 1980).

Two Probe Method

In contrast to the least squares method, the two probe method uses only two fixed probes. The measurements made are the two corresponding wave heights $2A_1$ and $2A_2$ and the phase difference $\delta = \delta_2$ between the two signals. These give rise to three equations for the three unknowns H, K_r, and β to be determined. Isaacson (1991) provides the corresponding solutions as:

$$a_i = \frac{1}{2|\sin\Delta|}\sqrt{A_1^2 + A_2^2 - A_1 A_2 \cos(\Delta + \delta)} \tag{3.21}$$

$$a_r = \frac{1}{2|\sin\Delta|}\sqrt{A_1^2 + A_2^2 - A_1 A_2 \cos(\Delta - \delta)} \tag{3.22}$$

$$\cos(\chi) = \frac{A_1^2 - a_i^2 - a_r^2}{2a_i a_r} \tag{3.23}$$

where $\Delta = \Delta_2$, $\delta = \delta_2$, and $\chi = 2kx_1 - \beta$. Once a_i and a_r are obtained from (3.21) and (3.22), H and K may then readily be obtained from (3.3) and (3.4); and once χ is obtained from (3.23), and β may be obtained as indicated by Eq. (3.20).

3.5.2 Regular Wave Transmission Analysis

The transmitted wave height is developed through energy passing a floating breakwater. This can occur through either one or a combination of the following: energy transmitted under the breakwater, energy transmitted over the breakwater (overtopping), diffraction between the ends of the breakwater and the flume walls and finally, a transfer of energy through the breakwater from its own motions. When considering the two-dimensional case in the flume, the gaps between the wall and the breakwater are kept to a minimum, therefore diffraction effects will be minimal and thus will not be considered in calculations. The process for analyzing the transmission coefficient is much less involved when compared to the reflection coefficient analysis. In fact, the transmission coefficient is obtained from the average wave height measurements from the two downwave probes. It is assumed that the reflected waves from the artificial beach are negligible and that the probes are sufficiently far from the breakwater for evanescent waves to be negligible. Therefore a reasonable approximation of the transmitted wave height was simply the average of the two recorded wave heights.

3.5.3 Energy Dissipation Coefficient

The energy dissipation coefficient K_e, is defined as the proportion of incident wave energy flux that is dissipated by the barrier or structure. A balance of energy flux requires that the energy flux of the incident wave train is equal to the energy flux of the transmitted and reflected wave trains, together with the energy flux that is dissipated. Since energy flux is proportional to wave height squared, the energy dissipation coefficient is expressed in terms of the reflection and transmission coefficients as:

$$K_e = 1 - K_r^2 - K_t^2 \tag{3.24}$$

where K_r and K_t are the reflection and transmission coefficients respectively.

3.5.4 Heave

The vertical motions of the floating breakwater were measured from videos taken of the experiments. A grid was placed on the flume as a measurement system for vertical heave motions. A reference dot was placed on both the model and the grid during steady state conditions which enabled a reasonable degree of accuracy in data acquisition. The peak-to-peak heave motions were measured by playing back the video, and these together with the incident wave heights were used to estimate the heave RAO's.

4.0 RESULTS AND DISCUSSION

The results from both the experimental and numerical analyses, which have been described in previous chapters, are discussed here. As indicated earlier, breakwater performance relating to the wave transmission, wave reflection, energy dissipation and breakwater heave motion will be considered whereas other important parameters of interest, including wave run-up and wave loads, will not be considered herein. The first section focuses on experimental results, the second section presents results from the numerical analysis and finally in the third section the experimental and numerical results are compared.

4.1 Experimental Results

A breakwater is considered a three-dimensional rigid body, thus it should have six degrees of freedom, namely: surge, heave, sway, roll, yaw and pitch as shown in Fig. 7. However, experiments conducted in the wave flume study the breakwater as a two-dimensional system with only the surge, heave and roll DOF's to consider. The restraining piles suppress the motion even further, constricting it in surge as well as in roll, leaving only heave.

One of the most important parameters in evaluating the effectiveness of a breakwater is the transmission coefficient. This was analyzed with wave probe results using the measured wave heights at each probe. Reflected waves from the beach were considered negligible and not included in the analysis. Transmitted wave results all follow a similar trend where the transmitted wave decreases in turn with the wave length.

Wave reflection was predominately estimated using the least squares method which considers the superposition of reflected waves with the incident waves. This entailed the consideration of water surface elevation measurements from all three probes on the upwave side of the breakwater. Results from the two probe method were used as a verification considering the possibility of the least square method failing. The resulting reflection coefficient graphs all show similar trends as K_r increases with ka. Higher K_r values are preferable since the most effective breakwaters are ones which have higher reflection and energy dissipation coefficients and smaller transmission coefficients. Slight dispersions in the data may be attributed to imperfections in the experiment itself, sensitivities of the reflected wave analysis and perhaps sloshing within the wave flume.

As stated previously in equation 3.36, energy dissipation is a direct result of the combined transmission and reflection coefficients, however the various components within the ongoing energy dissipation leave some room for speculation. Consider for example the friction losses due to the breakwater-pile interface as well as the breakwater-flume interface, where the prescribed gap occasionally makes the movements jerky and can cause large impulsive forces on the piles. Further energy losses may be attributed to wave sloshing in the flume and viscous effects around the breakwater corners. It is also noted that the energy dissipation coefficient is lower for smaller period waves, thus giving more accurate results at shorter wave periods.

The pile restrained floating breakwater treated in this study was a semi-fixed floating structure of which the sway, surge, yaw, roll and pitch modes were strongly constricted. This leaves the breakwater to essentially move freely in the vertical direction. Results tabulated for the heave motions show a strong correlation between the heave and both the gap between the piles and the wave steepness.

The performance of a pile restrained floating breakwater was tested as a semi-fixed floating breakwater by considering four situations: varying gap, varying steepness, freely-floating, and fixed. It has been indicated that improving the restraining system can reduce both the wave transmission and the floating body motions.

4.1.1 Incident Wave Results

A complete set of test wave conditions were reproduced in order to examine the incident wave field in the absence of any reflections from the breakwater. This was achieved by measuring incident waves for each of the 32 specified experimental cases using the five probe array. These tests were conducted before placing the breakwater in the flume, where one wave probe was fixed in its place so as to give accurate wave height characteristics at the breakwater location. The results from the wave probe showed the actual incident wave profiles to agree quite well with those specified.

The regular wave analysis was carried out using measurements of an initial portion of the record, before undesired wave energy reflected by the beach reached the wave probes. These precautions are taken to avoid possible errors in the results.

When the incident wave length L exceeds 10 or 15 times the breakwater beam B (i.e. when $B/L \leq 1/10$), the structure is essentially transparent to the waves. In the present study the maximum value of this ratio is $B/L = 1/8$. This ensures only the most optimum situations are being investigated.

4.1.2 Influence of Gap

Four sets of tests were conducted by varying the gap G between the breakwater and the piles set at G = 0 cm, 2 cm, 4 cm and 8 cm, while the wave steepness H/L was held constant at 0.05. Figures 8(a), 8(b) and 8(c) show the reflection coefficient, transmission coefficient and the energy dissipation coefficient respectively as functions of ka for all four gaps, while Figs. 9(a), 9(b) and 9(c) show the reflection, transmission and energy dissipation coefficients as functions of the gap G for various values of ka. Here a is half of the breakwater beam, (i.e. $a = B/2$).

The transmitted wave height is a parameter of utmost importance in the analysis of a breakwaters' effectiveness. If the transmitted wave height is not reduced a reasonable amount from the incident wave height, the efficiency of the breakwater essentially becomes negligible. Figure 8(a) shows the transmission coefficient as it exhibits a downward trend as ka is increased. The experimental values range from about 0.8 to 0.9 at ka = 0.2 to about 0.1 to 0.3 at ka = 0.9. Reasonable attenuation of incident waves through both wave reflection and energy dissipation is concluded from this particular pile restrained set-up.

The reflection coefficient K_r shown in Fig. 8(b) exhibits the opposite trend to the transmission coefficient tendencies as expected. Here, K_r generally increases as ka is increased, with values of K_r varying from 0.1 to 0.9. The influence of the gap on the reflection coefficient is also seen in this figure with the largest gap G = 8 cm corresponding to lower wave reflection when compared to other gap spacings.

The energy dissipation coefficient K_e was defined previously by:

$$K_e + K_r^2 + K_t^2 = 1 \tag{4.1}$$

On this basis, measured values of K_t and K_r have been used to determine the energy dissipation coefficient. Values shown in Figs. 8(c) and 9(c) display K_e ranging from 0 to 0.4 in both cases.

Figure 9 contains the same data as in Fig. 8, but the coefficients are now plotted as functions of G for various values of ka. Figure 9 shows reasonably constant values of K_t and K_r as the gap spacing is changed, so that the magnitude of the gap is expected not to unduly influence the transmission characteristics of the breakwater.

The influence of a varying gap on heave motions is shown in Fig. 10. This figure depicts a distinguishable correlation between the gap spacing and the resulting heave motions. Movements of an essentially fixed breakwater should be zero, and thus are not shown on this figure. For a gap G = 2 cm, the heave RAO was between 0.25 and 0.8, for a gap G = 4 cm, the heave RAO was in the range 0.6 to 0.8, and finally for a gap G = 8 cm, the heave RAO fell between 0.55 and 0.95. The higher heave RAO's for the largest gap are estimated to be a result of increased lateral movements, including roll and surge, which are permitted by the experimental set up. The friction between the breakwater and the piles may constrict the heave motion to some extent but also note that the roll motion cannot be perfectly fixed as long as heave motion is allowed. This requires that the pile-supported breakwater be subjected to restoring forces due to the friction in the heave and roll modes of motion, whereas the sway motion is almost fully restricted.

4.1.3 Influence of Wave Steepness

The influence of wave steepness H/L was examined by conducting three sets of tests with three different values of steepness, H/L = 0.02, 0.05 and 0.08, all with a constant gap G = 4 cm. These tests evaluated the transmission coefficient, reflection coefficient, energy dissipation coefficient and heave RAO's. Figures 11(a), 11(b) and 11(c) show the transmission coefficient, reflection coefficient and the energy dissipation coefficient respectively as functions of ka for all three cases of steepness. Figure 12, which derives from the same data, shows these coefficients as functions of wave steepness for the various values of ka.

Figure 11(a) presents the transmission coefficients which have an inverse relationship with the reflection coefficients. A decrease in K_t values are observed as ka is increased, supporting the expected downward trend in transmission results. This decrease occurs as H/L is increased, subsequently causing the wave velocity also to increases and in turn energy dissipation increases. As more energy is dissipated from the system, the wave transmission is consequently decreased. Values for K_t range from 0.15 to 0.9 for various steepness conditions. It is clear from experimental results that the transmission coefficient is influenced by variations in wave length, wave height and gap distance between the breakwater and the piles

The influence of steepness on the reflection coefficient K_r is seen in Fig. 11(b). The anticipated increasing trend of K_r with ka is confirmed once again with the measured results. Reflection values corresponding to an H/L of 0.02 shows K_r to be increasing from 0.4 to 0.95, an H/L of 0.05 gives a K_r value between 0.45 and 0.9, and lastly an H/L of 0.08 shows K_r to range from 0.5 to 0.9.

Energy dissipation coefficient K_e derives from the measured values of K_t and K_r. Experimental results show K_e values ranging from 0 to 0.55 for the three steepness values with respect to ka shown in Fig. 11(c). The highest energy dissipation values occur during an H/L = 0.08 where the waves are quite steep with wave heights reaching a maximum of 20 cm.

Similar to Fig. 11, Fig. 12 portrays the three hydrodynamic coefficients as functions of wave steepness while varying ka. Figure 12(a) indicates values of K_t have a moderate decrease with respect to increasing values of H/L, consequently, as ka increases, the transmission coefficient decreases.

Figure 12(b) presents K_r as a function of H/L with varying ka values. The tendency exhibited here includes a rather uniform K_r value, perhaps increasing slightly when plotted against H/L. The inclination here, as ka increases, is a subsequent increase in the reflection coefficient.

Alternatively, K_e is graphed as a function of H/L, as ka values are varied, in Fig. 12(c). This shows a consistent tendency of K_e vs. wave steepness for varying values of ka.

The influence of wave steepness on the resulting vertical breakwater motions are shown in Fig. 13. Heave RAO's have been computed and are seen to follow a trend which correlates the increases in wave steepness with the breakwater heave motions. The breakwater heave RAO's for a steepness H/L of 0.02 range from 0.7 to 0.9, for an H/L of 0.05 heave RAO's are between 0.6 and 0.8, and finally for an H/L value of 0.08, heave RAO's are about 0.3 to 0.6. An appreciable decrease is seen from the heave values shown here between H/L = 0.05 and H/L = 0.08. This could be the result of potential roll and sway motions as the waves become much steeper and thus, causing influential forces on the piles with an increase in jerking motions.

4.1.4 Fixed Breakwater

Tests were conducted with the model breakwater restrained by vertical piles in which the gap between the breakwater and the piles was incrementally decreased. When this gap reached zero the situation was essentially fixed. The corresponding results for the fixed case are shown in Fig. 14. The two different wave steepnesses that were considered are firstly, an H/L of 0.02 and secondly, an H/L of 0.05.

Figure 14(a) illustrates the behaviour of the transmission coefficient with ka for both H/L values. The results show a decreasing trend of K_t as ka increases. This experimental data provides values of the fixed transmission coefficient quite similar to those of the pile restrained transmission coefficients. Transmission values range from about 0.3 to 0.9 in both cases.

The reflection coefficient is plotted in Fig. 14(b) with ka for both H/L values. The results show similarities to previous experimental results as K_r increases with ka. A wave steepness H/L of 0.02 gives values slightly lower than those of the higher wave steepness H/L of 0.05. The range for reflection coefficient values in both H/L cases is between 0.02 and 0.95.

The energy dissipation coefficient is shown as a function of ka in Fig. 14(c). An ideal situation would give rise to an energy dissipation coefficient of zero, however, here we have values of K_e increasing up to = 0.7 for H/L = 0.02 and up to 0.4 for H/L = 0.05. The energy dissipation coefficient is essentially a data error term, therefore, we can see slightly higher errors in this section.

Heave results for the fixed case have not been shown graphically since they are logically zero for all cases. However there was slight movement in the breakwater at the largest wave period and steepness because of the inadequacies and limitations of the restraining system for such conditions.

4.1.5 Freely Floating Breakwater

Experimental tests with a freely floating breakwater were conducted by attaching a loose elastic band from the flume rails to the breakwater simply to prevent extensive drift motions, while allowing movement in all six directions, namely, sway, surge, yaw, roll, pitch and heave. The steepness was kept constant at 0.02 as the wave period was incrementally increased.

Transmission coefficient results for the for the freely floating case are shown in Fig. 15(a) and exhibit a general similarity to previous data. The transmission coefficient decreases as ka increases with values fluctuating from a K_t of 0.35 to 0.8. These values are slightly higher, on average, than for the pile restrained and fixed cases which may be a result of higher breakwater motions producing larger transmitted waves.

The analysis of reflection coefficient results for the freely floating case lead to the same expected tendency as in the case of a varying gap and wave steepness. The general trend, shown in Fig. 15(b), ensues an increase in the reflection coefficient (K_r), as ka increases. These values are much lower when compared to the pile restrained case, ranging from a K_r of 0.15 to 0.55.

Figure 15(c) presents the energy dissipation coefficient as a function of ka, where values range from a K_e of 0.15 to 0.6, which are similar to the energy dissipation results from the pile restrained case. The heave RAO was found to be unity in almost all cases and is therefore not shown graphically.

4.2 Numerical Results

The HAFB model, discussed in chapter 2, was used to numerically evaluate the hydrodynamic coefficients simulating the experimental set-up. Input values were representative of the experimental procedure including breakwater dimensions, wave period, mooring stiffness and viscous damping. Data analysis was conducted for three different cases. The first was a varying stiffness matrix representing a fixed case, freely floating case and for comparison with experimental results, a stiffness matrix constricted strongly in the surge, sway, roll, pitch and yaw modes leaving essentially free movement only in the heave direction with results presented in Fig. 16. The second set of numerical results were generated by varying the breakwater draft and are presented in a non-dimensional form of B/h in Fig. 17. Finally, the damping coefficient and its effects on wave transmission, reflection, energy dissipation, and force is explored in Figs. 18.

A general feature of floating breakwaters is the strong dependence of wave transmission on wave length and wave steepness. This dependence has been demonstrated in models many times, confirmed by field experience and has also been validated by this present study. The prototype used in the experimental testing stage was simulated numerically where efficiencies between numerical and experimental results were evaluated and compared. Numerical analysis gave rise to three sets of data being generated with varying conditions in each.

4.2.1 Experimental Simulation

In this section, numerical results are explored which were modeled as closely as possible to experimental testing conditions. These include the pile restrained case, the freely floating and the fixed scenarios with periods ranging from 0.8 to 2.0 s accompanied by corresponding stiffness matrices representing each situation.

The transmission coefficient for the simulated pile restrained case, shown in Fig. 16(a), produced values near one for long waves and dropped down to 0.45 for a shorter waves having a period of 0.8 s. Both the fixed and freely floating transmission coefficient results are also plotted on this figure, consistently following the expected trend where the transmission coefficients decrease with lower wave periods. Included in the freely floating case is the consideration of added mass .

The numerical reflection coefficient results for the pile restrained, freely floating and fixed cases, are presented in Fig. 16(b). This figure is essentially the inverse of Fig. 16(a) where the reflection coefficient values range from zero and gradually increase up to 0.9 as the wave period decreases to 0.8 s (increasing ka).

Energy dissipation coefficient is derived from a relationship including both the reflection and transmission coefficients. The energy dissipation coefficient essentially follows a uniform trend tending toward zero in an ideal situation. Discrepancies in this value, straying from zero, explain energy losses which are essentially error terms in the data analysis.

4.2.2 Variation in Draft

Results were obtained for a replicated set of parameters similar to those in the experimental case, with the exception of a varied draft. In the experimental case, the draft was held constant at 0.1 m whereas the numerical analysis encompassed variations from 0.08, 0.1, 0.12 to 0.14 m. The corresponding results for the transmission and reflection coefficients are shown as functions of B/h in Fig. 17.

The transmission coefficients, which are displayed in Fig. 17(a), are essentially unity over the lower ka region, corresponding to higher wave periods, and decrease as ka increases. A definite dependence on relative breakwater draft is seen, with an increased draft leading to a decrease in the transmission coefficient, particularly at higher ka values (shorter waves).

The reflection coefficient, shown in Fig. 17(b), exhibits an inverse trend to the transmission results giving estimates close to zero at lower ka values, and increasing at higher ka values up to almost 1.0.

The energy dissipation coefficient was determined using equation (2.5), with results of essentially zero throughout since viscous damping was assumed.

4.2.3 Variation in Damping

Changes to the level of viscous damping were investigated in the numerical model, in part to asses suitable values for reproducing the experimental results. Four different damping ratios were considered in the numerical model: 0, 0.05, 0.10 and 0.15. Figure 18 presents the corresponding results.

Figure 18(a) shows that the transmission coefficient decreases monotonically as the damping ratio is increased. These numerical results confirm the expected tendency of a well-behaved transmitted wave past the breakwater with transmission coefficient values ranging from about 0.3 to 1.0.

Figure 18(b) shows the reflection coefficient as the damping is varied. Results indicate a tendency toward the inverse of the transmission coefficient figure, however, an ideal monotonic representation is not apparent. The analysis involved in determining reflection coefficients is a more difficult process than the predictions involved in defining transmissions coefficients.

4.3 Comparison of Experimental and Numerical Results

Figure 19 shows a comparison of numerical and experimental results of hydrodynamic coefficients for the pile restrained case, presenting both transmission and reflection coefficients varying with ka. The correlation between the two predictions show that the numerical model gives more conservative results, i.e. transmission coefficients are generally higher and reflection coefficients are generally lower, when compared to actual experimental hydrodynamic motions.

Figure 20 explores the vertical heave motions of the floating breakwater in terms of a response amplitude operator. Once again, the numerical model generally gives conservative estimates, where heave motions were numerically predicted to be somewhat higher than those actually found in the experiments. The highest heave RAO values for the numerical freely floating case tend toward unity whereas the lowest values are zero in the fixed case. Heave values have been non-dimensionalized with the wave height, H/2 and are given in tables 1 through 4 for experimental results.

Finally, the numerical and experimental results are compared in Figs. 21 and 22 for the fixed and freely floating cases respectively. Both the fixed case and freely floating case show numerical predictions to be generally conservative where numerical transmission coefficients are generally higher than experimental results and numerical reflection coefficients are generally lower than those predicted experimentally.

5.0 CONCLUSIONS AND RECOMMENDATIONS

The performance of a pile restrained floating breakwater has been analyzed through both an experimental program and numerical examination. Results have shown that the performance of a floating breakwater is significantly influenced by its restraining mechanism. The flexibility of the mooring, in terms of restraint, controls the motion of the breakwater and hence the relative magnitude of waves generated by the breakwater and the energy dissipated through turbulence. A fixed structure, is expected to reduce transmitted waves, however it experiences increased mooring forces In contrast, a freely floating structure would permit increased transmitted waves but the system experiences minimal mooring forces. Conceivably an optimum system lies between these two extremes. This is where the semi-restrained floating breakwater is evidently appropriate, and has been considered and compared with the freely floating and fixed systems.

Experimental work conducted in this study tested the breakwater in three ways: freely floating, fixed and semi-fixed allowing movement in primarily the heave direction. These tests were carried out using a constant water depth for a series of regular wave conditions with varying wave periods, wave steepnesses, and gap spacing between the piles and the breakwater. The reflected wave heights were estimated using a least squares method applied to the measurements of the water surface elevation, whereas the transmitted wave heights were estimated simply by using the wave height measurements directly and neglecting the reflection from the beach. Heave RAO's were established directly from video records.

Results from the diverse set of gap spacings tend to point toward an optimum situation at a gap G of 2 cm. This is where both the transmitted waves and the breakwater heave reach a minimum. As the wave steepness was varied, it appears that at a value H/L of 0.05, the poorest results are generated, i.e. the transmission coefficient is higher than that of H/L = 0.02 and H/L = 0.08. Although the most efficient results come from H/L = 0.08 with respect to transmission, the heave values are unfortunately at their peak here.

The correlation between results may contain slight inconsistencies due to certain experimental error, thus it is recommended that further study be conducted in this area with a more extensive program of tests in order to confirm the present results and to verify, more solidly, the general trend. Further study should also necessitate both directional variations and random wave effects, and ideally, the implementation of a field study would be most beneficial, in order to validate both the experimental and numerical analysis described herein.

Numerical results for the transmitted waves, reflected waves and heave motions have been computed using the program HAFB which is based on linear potential theory to predict wave loads and motions of a floating breakwater in oblique seas. Three sets of results were obtained: the first incorporated three different mooring stiffness matrices which were altered to simulate pile restrained (heave motions only), freely floating and fixed cases, secondly, the breakwater draft was varied and is presented in a non-dimensional form of B/h, and finally the damping coefficients were varied and their effects on wave transmission, wave reflection and energy dissipation is explored. Numerical results have shown reasonable correspondence with experimental results. Results for the pile restrained, fixed and freely floating stiffness matrices show transmission coefficients to follow the expected downward trend and inversely, the reflection coefficients increase with ka. However, more discrepancies are seen in the reflection coefficient results since the reflected wave train is expected to have a more sensitive system as it mixes with incident wave trains. The results also indicate that an increase in relative draft provokes a monotonic decrease in the transmission coefficients and essentially the inverse is true for the reflection coefficient as it increases with increasing ka values. Finally, an increase in damping gives rise to decreasingly lower wave transmission values and increasingly higher wave reflection values.

6.0 REFERENCES

Adee, B.H. (1976). "Floating breakwater performance." *15th Proceedings of the Coastal Engineering Conference.* ASCE, Honolulu, HI. Vol. 3, pp. 2777-2791.

Agerton, D.J., Savage,G.H., Stotz, K.C. (1976). "Design, analysis and field test of a dynamic floating breakwater." *15th Proceedings of the Coastal Engineering Conference.* ASCE, Honolulu, HI. Vol. 3, pp. 2792-2809.

Aoki, S-I., Kim, H-T., Sawaragi, T. (1994). "Wave control by pile-supported floating breakwaters." *Proceedings of the 4th (1994) International Offshore and Polar Engineering Conference*, Osaka, Japan. Vol. 3, pp. 545-549.

Blumberg, G. P., Cox, R. J. (1988). "Floating breakwater physical model testing for marina applications." *Bulletin of the Permanent International Association of Navigation Congresses.* No. 63, pp. 5-13.

Black, J. L., Mei, C. C., Bray, C. G. (1971). "Radiation and scattering of water waves by rigid bodies." Journal of Fluid Mechanics, 46(1), pp. 151-164.

Christian, C.D. (1993). "Motions of floating breakwaters." *11th Australasian Conference on Coastal and Ocean Engineering.* Townsville, Queensland, pp. 295-299.

Fraser, G. (1979). "Dynamic response of moored floating breakwaters." M.A.Sc. Thesis, Dept. of Civil Engineering, University of British Columbia, Vancouver, B.C.

Gaythwaite, J.W. (1987). "Floating breakwaters for small craft facilities." *Civil Engineering Practice*, Vol. 2, No. 1, pp. 89-108.

Gaithwaite, J. W. (1988). "Practical aspects of floating breakwater design. *Bulletin of the Permanent International Association of Navigational Congresses.* No. 63, pp. 31-49.

Isaacson, M. (1991). "Measurement of regular wave reflection." *Journal of Waterway, Port, Coastal and Ocean Engineering*, ASCE, Vol. 117, No. 6, pp. 479-491.

Isaacson, M., Byres, R. (1988). "Floating breakwater response to wave action." *Proceedings of the 21st International Conference on Coastal Engineering.* Costa del Sol, Spain, ASCE, Vol. 3, pp. 2189-2200.

Isaacson, M., Nwogu, O. U. (1987). "Wave loads and motions of long structures in directional seas." *Journal of Offshore Mechanics and Arctic Engineering*, Vol. 109, pp. 126-132.

Kennedy, A.B. (1993). "Small craft motion in reflected, long-crested seas." M.A.Sc. Thesis, Dept. of Civil Engineering, University of British Columbia, Vancouver, B.C.

McCartney, B.L. (1985). "Floating breakwater design." *Journal of Waterway, Port, Coastal and Ocean Engineering*, ASCE, Vol. 111, No. 2, pp. 307-317.

Miles, M. D. (1989). "User Guide for GEDAP Version 2.0 Wave Generation Software." *Hydraulics Laboratory Technical Report No. LM-HY-034*, National Research Council, Ottawa, Canada.

Moore, W.I., Sethness, E.D. (1986). "Design concepts for floating breakwaters." Ports '86. *Proceedings of a Specialty Conference on Innovations in Port Engineering and Development in the 1990's*, pp. 179-191.

Niwinski, C.T. (1982). "Nonlinear wave forces on floating breakwaters." M.A.Sc. Thesis, Dept. of Civil Engineering, University of British Columbia, Vancouver, B.C.

Pelletier, D. (1989). "Real Time Control System (RTC) User's Manual." *Hydraulics Laboratory Technical Report No. LM-HY-033*, National Research Council, Ottawa, Canada.

Sarpkaya, T., Isaacson, M., (1981). "Mechanics of wave forces on offshore structures." Van Nostrand Reinhold, New York.

Sorensen, R. M. (1978). "Basic coastal engineering." John Wiley & Sons, New York.

Werner, G. (1988). “Experiences with floating breakwaters: a literature review.” *Bulletin of the Permanent International Association of Navigation Congresses.* No. 63 pp. 23-30.

Yao, G., Ma, Z., Bingcan, D. (1993). “Experimental study on rectangular floating breakwaters.” *China Ocean Engineering*, China Ocean Press, Vol. 7, No. 3, pp. 323-332.

Appendix A

Experimental Results Tabulated

Table 1. Experimental Results for a Pile Restrained Breakwater with Various Gaps (H/L = 0.05).

T (sec)	G (cm)	L (m)	K_t	K_r	K_e	Heave RAO
0.8	0.0	1.00	0.270	0.960	0.006	0.000
1.2	0.0	2.06	0.777	0.320	0.294	0.000
1.4	0.0	2.58	0.477	0.594	0.420	0.000
1.8	0.0	3.56	0.826	0.557	0.008	0.337
0.8	2.0	1.00	0.120	0.869	0.230	0.240
1.2	2.0	2.06	0.743	0.475	0.223	0.777
1.4	2.0	2.58	0.651	0.664	0.135	0.775
1.8	2.0	3.56	0.879	0.260	0.159	0.730
0.8	4.0	1.00	0.180	0.918	0.125	0.600
1.2	4.0	2.06	0.752	0.821	0.283	0.816
1.4	4.0	2.58	0.705	0.657	0.071	0.775
1.8	4.0	3.56	0.893	0.466	-	0.787
0.8	8.0	1.00	0.150	0.812	0.318	0.520
1.2	8.0	2.06	0.874	0.101	0.226	0.932
1.4	8.0	2.58	0.678	0.567	0.218	0.744
1.8	8.0	3.56	0.879	0.534	-	0.697

Table 2. Experimental Results for a Pile Restrained Breakwater with Various Wave Steepnesses, (G = 4 cm).

T (sec)	H/L	L (m)	K_t	K_r	K_e	Heave RAO
0.8	0.02	1.000	0.250	0.987	-	0.800
1.0	0.02	1.210	0.467	0.590	0.434	0.800
1.2	0.02	2.052	0.732	0.681	0.001	0.878
1.4	0.02	2.574	0.667	0.426	0.374	0.823
1.6	0.02	3.078	0.581	0.396	0.506	0.742
1.8	0.02	3.568	0.873	0.617	-	0.845
2.0	0.02	4.078	0.707	0.459	0.289	0.927
0.8	0.05	1.000	0.180	0.918	0.125	0.600
1.2	0.05	2.060	0.752	0.821	0.283	0.840
1.4	0.05	2.580	0.705	0.657	0.071	0.775
1.8	0.05	3.560	0.893	0.466	-	0.787
0.8	0.08	1.000	0.169	0.932	0.103	0.300
1.2	0.08	2.050	0.421	0.508	0.565	0.610
1.4	0.08	2.575	0.400	0.577	0.507	0.631

Table 3. Experimental Results for a Fixed Breakwater.

T (sec)	H/L	L (m)	K_t	K_r	K_e
0.8	0.02	1.000	0.300	0.945	0.017
1.0	0.02	1.210	0.433	0.530	0.531
1.4	0.02	2.574	0.490	0.277	0.683
1.6	0.02	3.078	0.508	0.537	0.453
1.8	0.02	3.568	0.894	0.228	0.149
0.8	0.05	1.000	0.270	0.960	0.006
1.2	0.05	2.060	0.777	0.320	0.294
1.4	0.05	2.580	0.477	0.594	0.420
1.8	0.05	3.560	0.826	0.557	0.008

Table 4. Results for a Freely Floating Breakwater (H/L = 0.02).

T (sec)	L (m)	K_t	K_r	K_e	Heave RAO
0.8	1.000	0.350	0.554	0.571	1.000
1.0	1.210	0.550	0.392	0.544	1.000
1.2	2.052	0.829	0.422	0.134	1.000
1.4	2.574	0.814	0.350	0.215	1.000
1.8	3.568	0.838	0.163	0.271	0.901
2.0	4.078	0.616	0.169	0.592	0.976

FIGURES

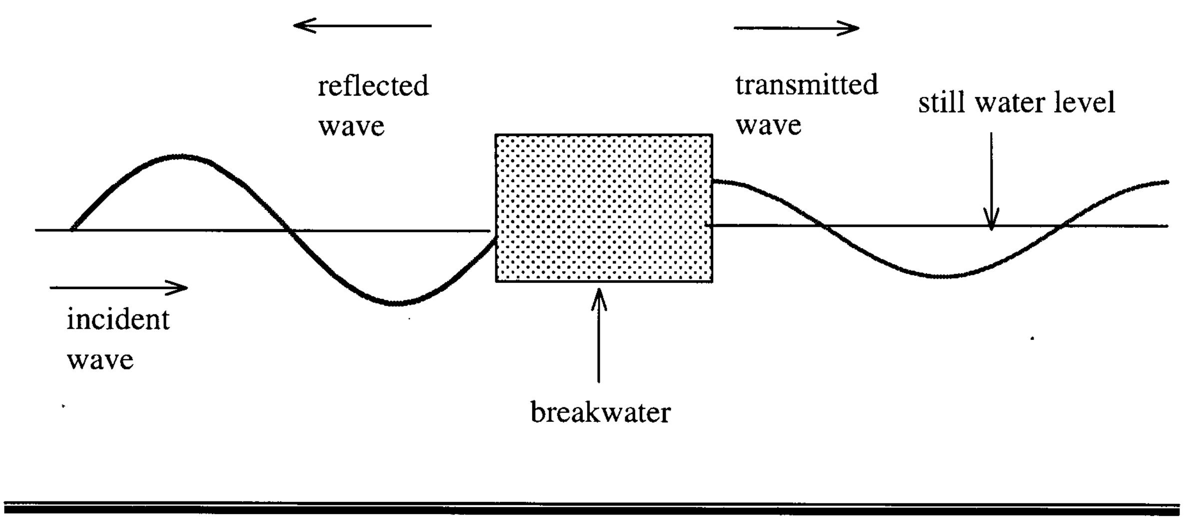

Figure 1. Sketch of a floating breakwater subjected to an incident wave.

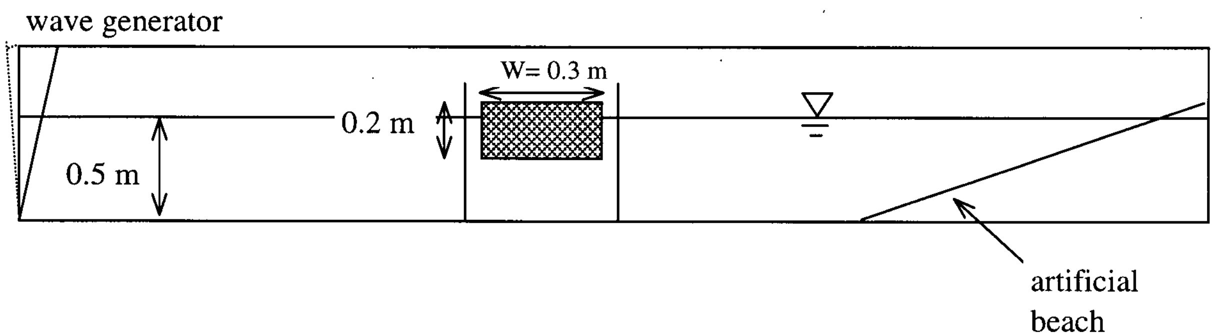

Figure 2. Definition sketch of experimental set-up.

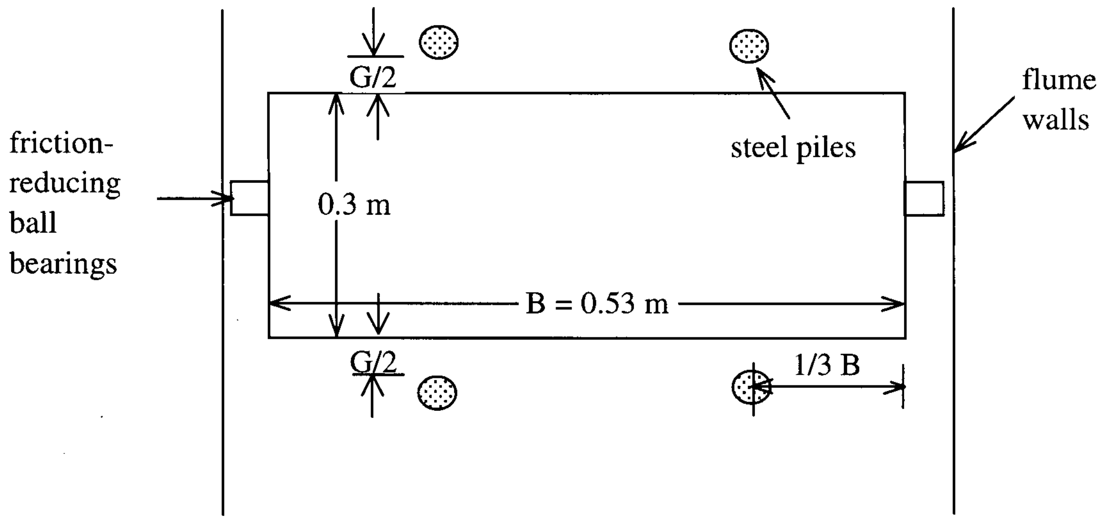

(a)

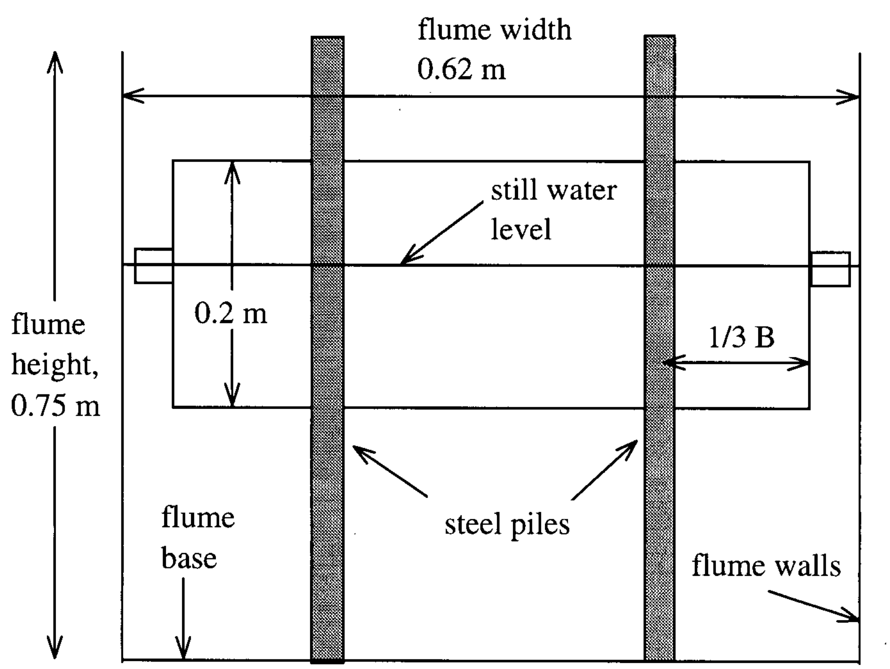

(b)

Figure 3. Definition sketch of breakwater fixed with vertical piles. (a) Plan view, (b) front view.

Figure 4. Photograph of wave flume looking toward the beach.

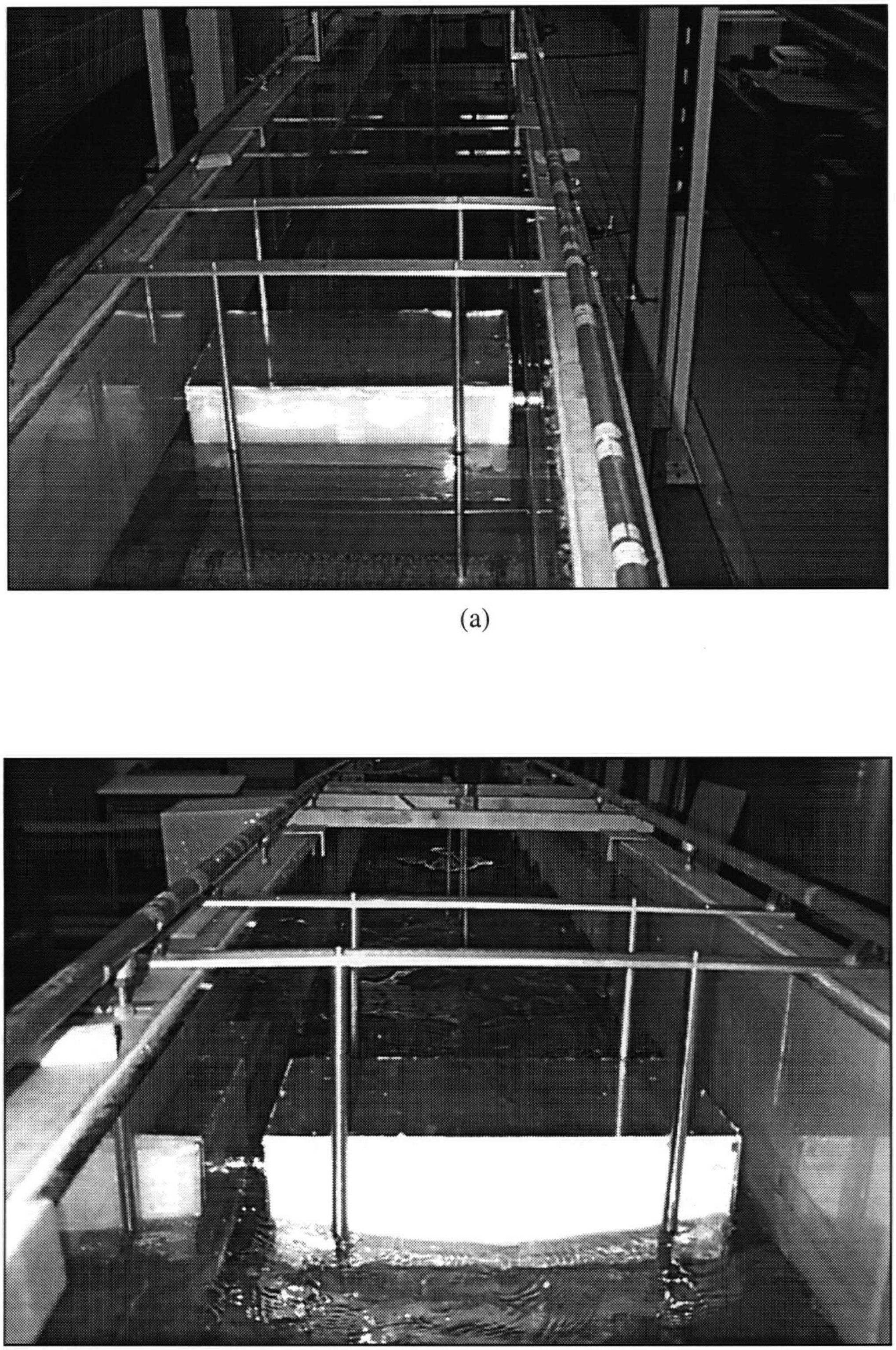

(a)

(b)

Figure 5. Photographs of breakwater restrained with vertical piles. (a) looking downwave, (b) looking upwave.

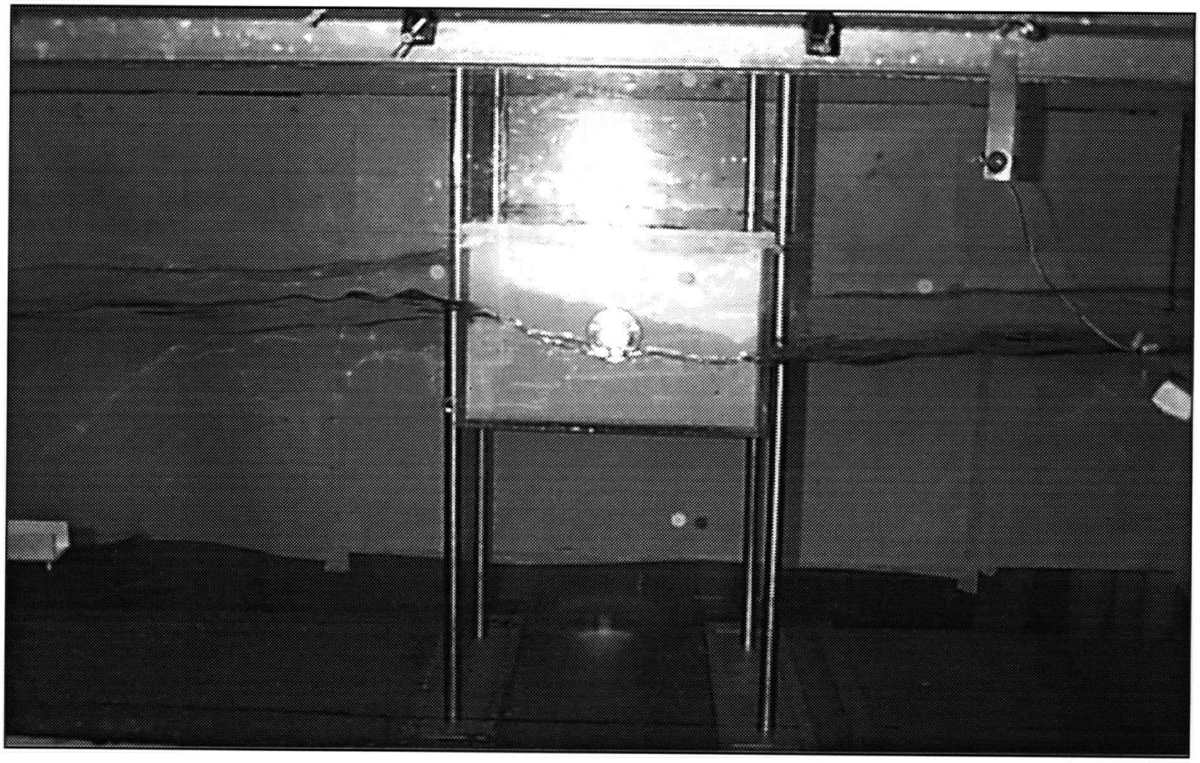

Figure 6. Side view photograph of pile restrained breakwater.

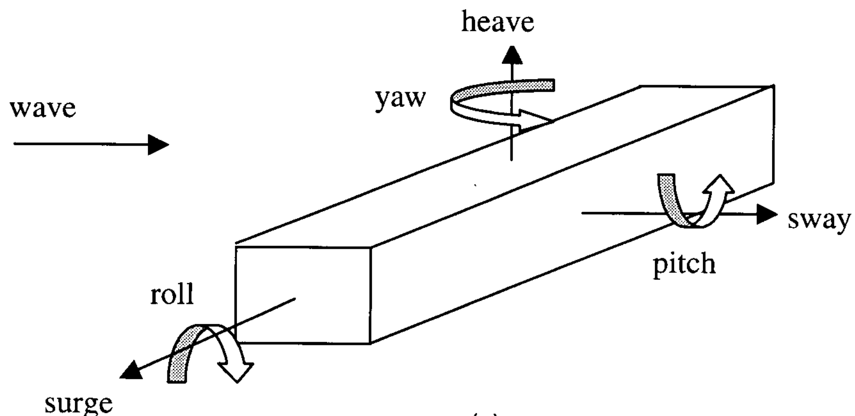

Figure 7. A breakwaters' six degrees of freedom.

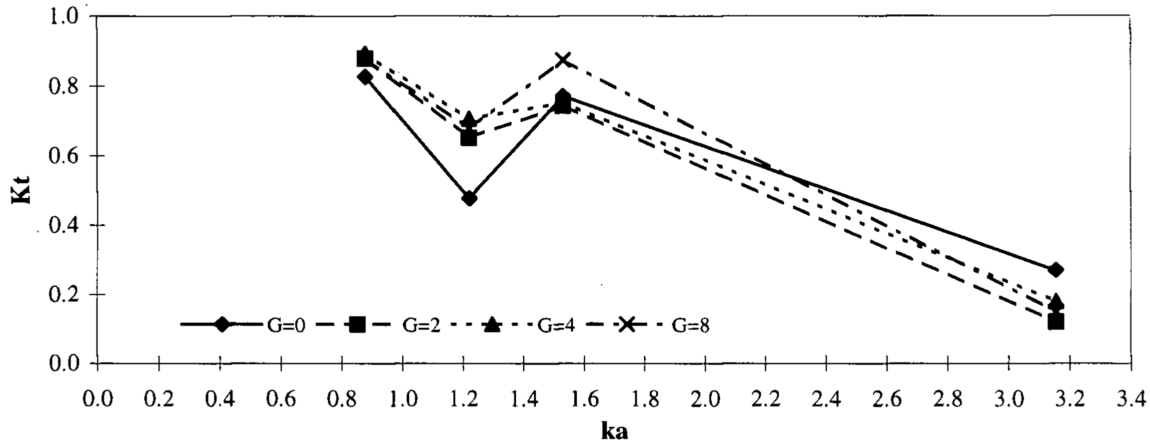

(a)

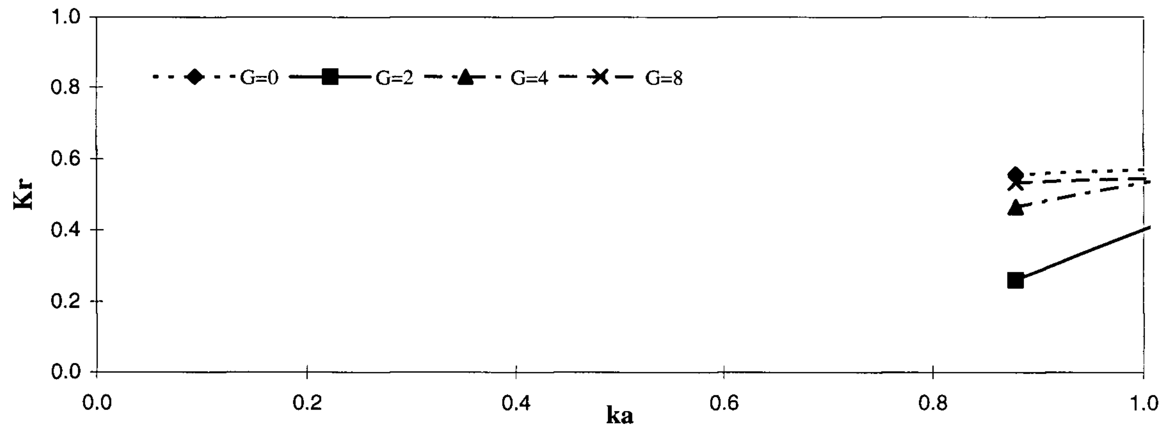

(b)

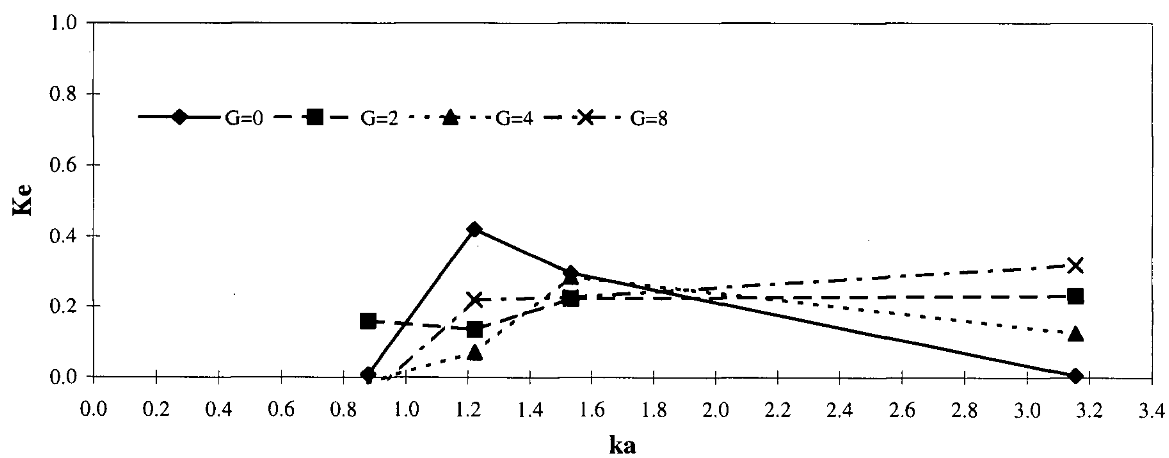

(c)

Figure 8. Hydrodynamic coefficients as a function of ka for varying gap (G in cm) for the pile restrained case. (a) transmission coefficient, (b) reflection coefficient, (c) energy dissipation coefficient.

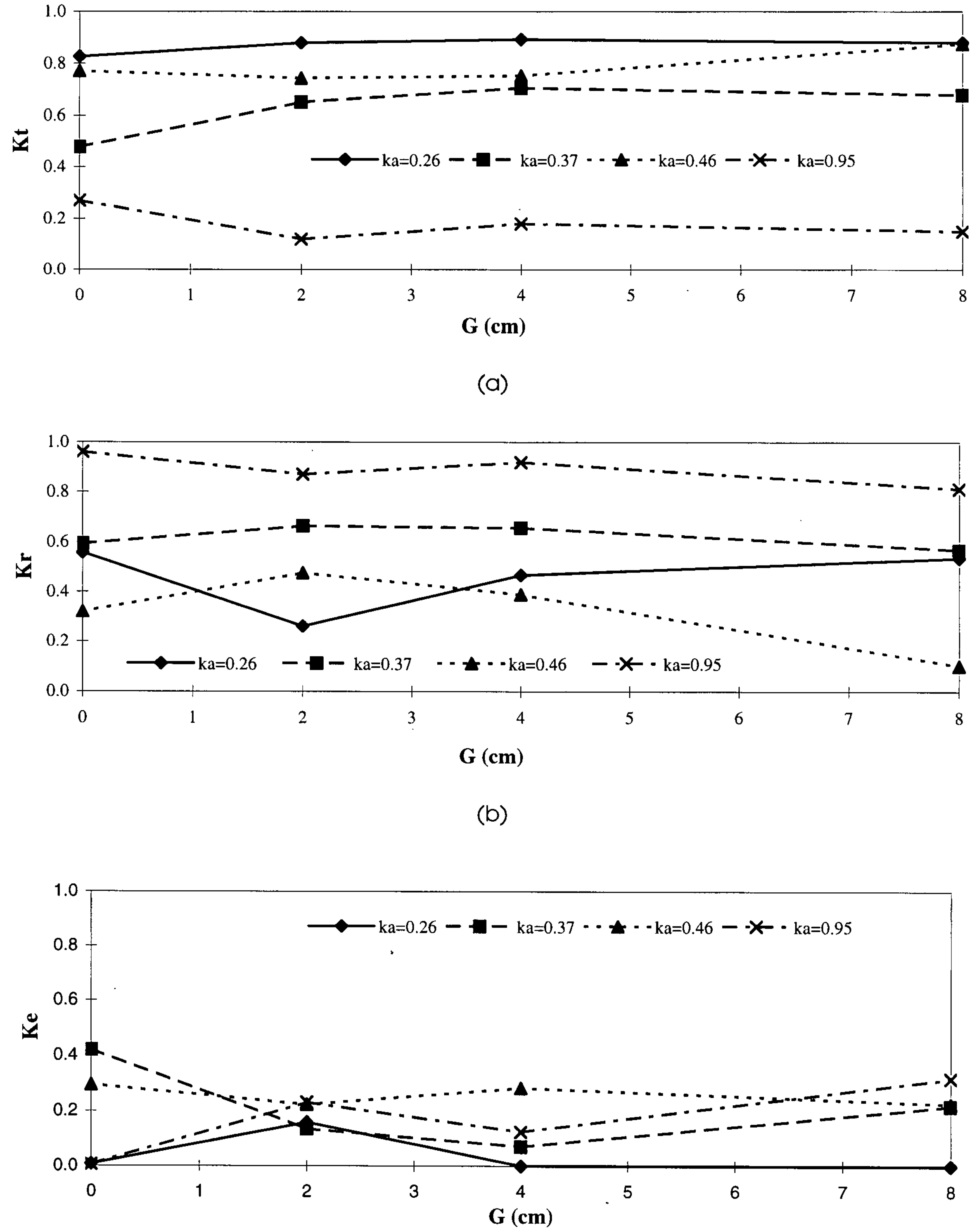

(c)

Figure 9. Hydrodynamic coefficients as a function of gap with varying ka for the pile restrained case. (a) transmission coefficient, (b) reflection coefficient, (c) energy dissipation coefficient. Constant steepness, H/L = 0.05.

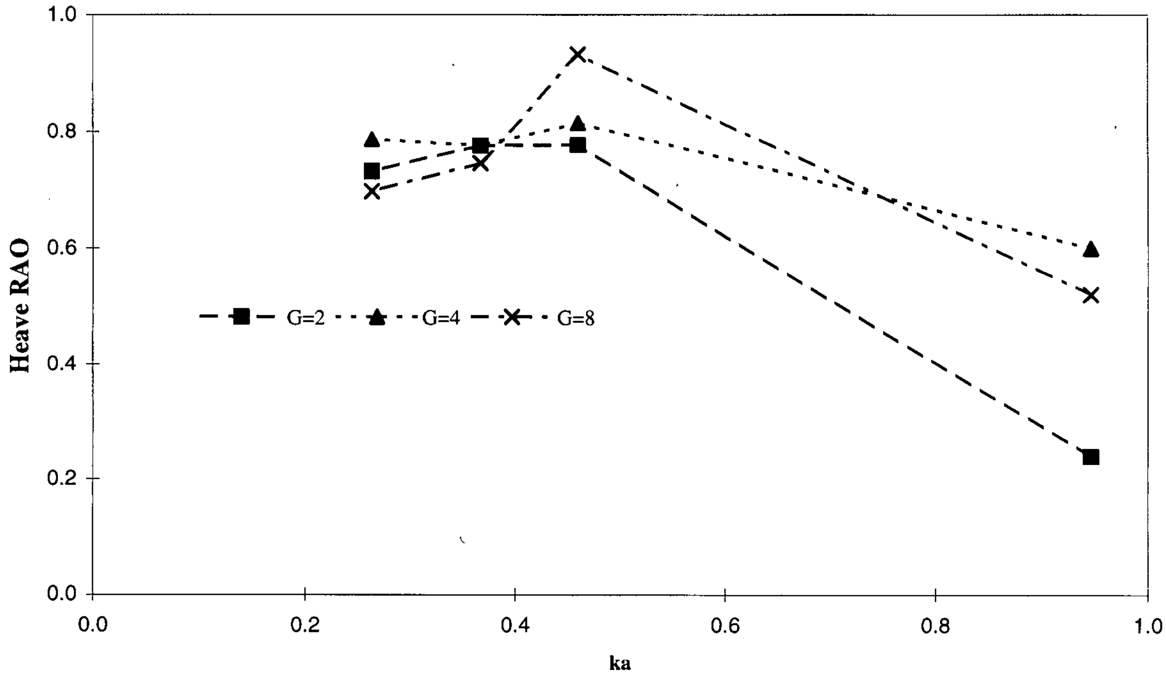

Figure 10. Heave response amplitude operator's as a function of ka for a varying gap spacing.

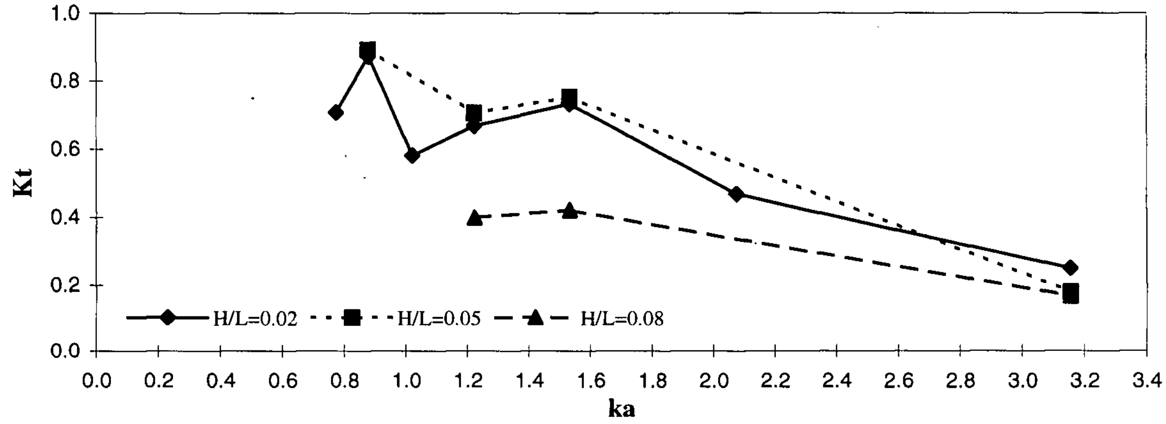

(a)

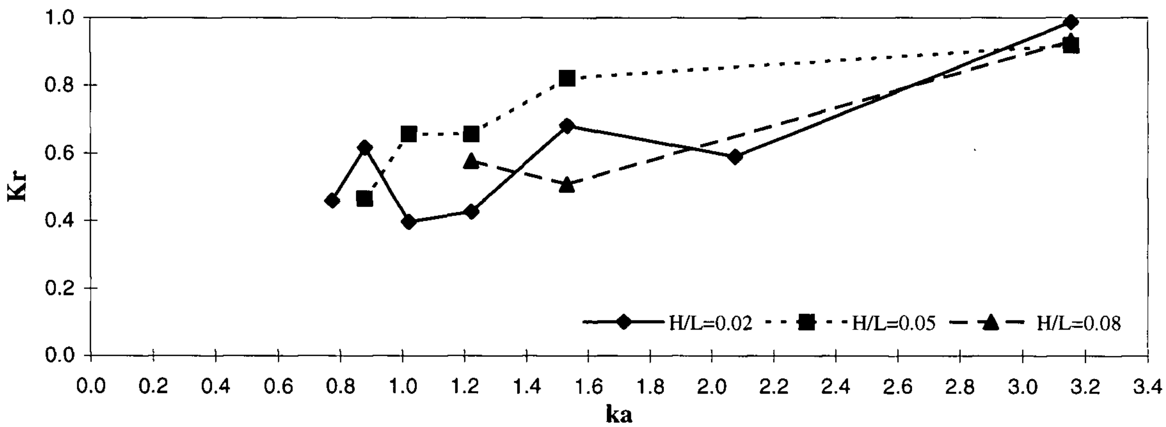

(b)

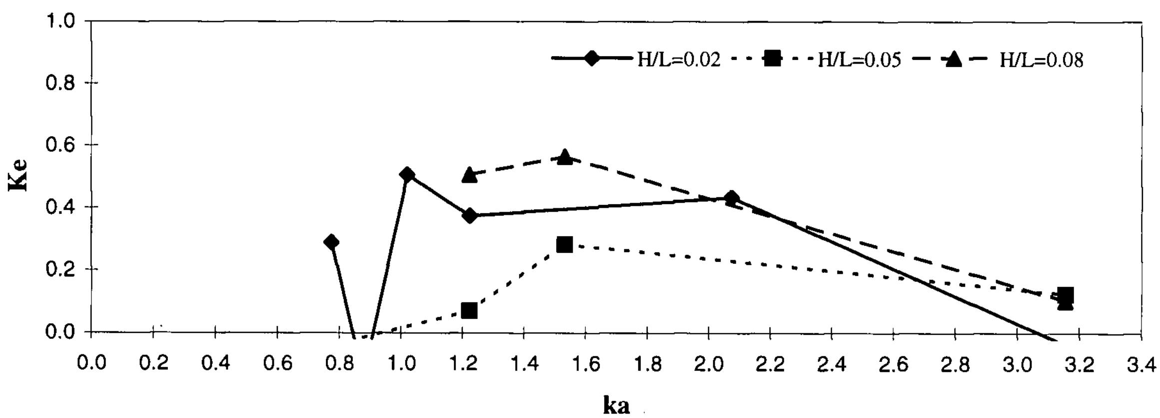

(c)

Figure 11. Hydrodynamic coefficients as a function of ka with varying wave steepness, H/L, for the pile restrained case. (a) transmission coefficient, (b) reflection coefficient, (c) energy dissipation coefficient.

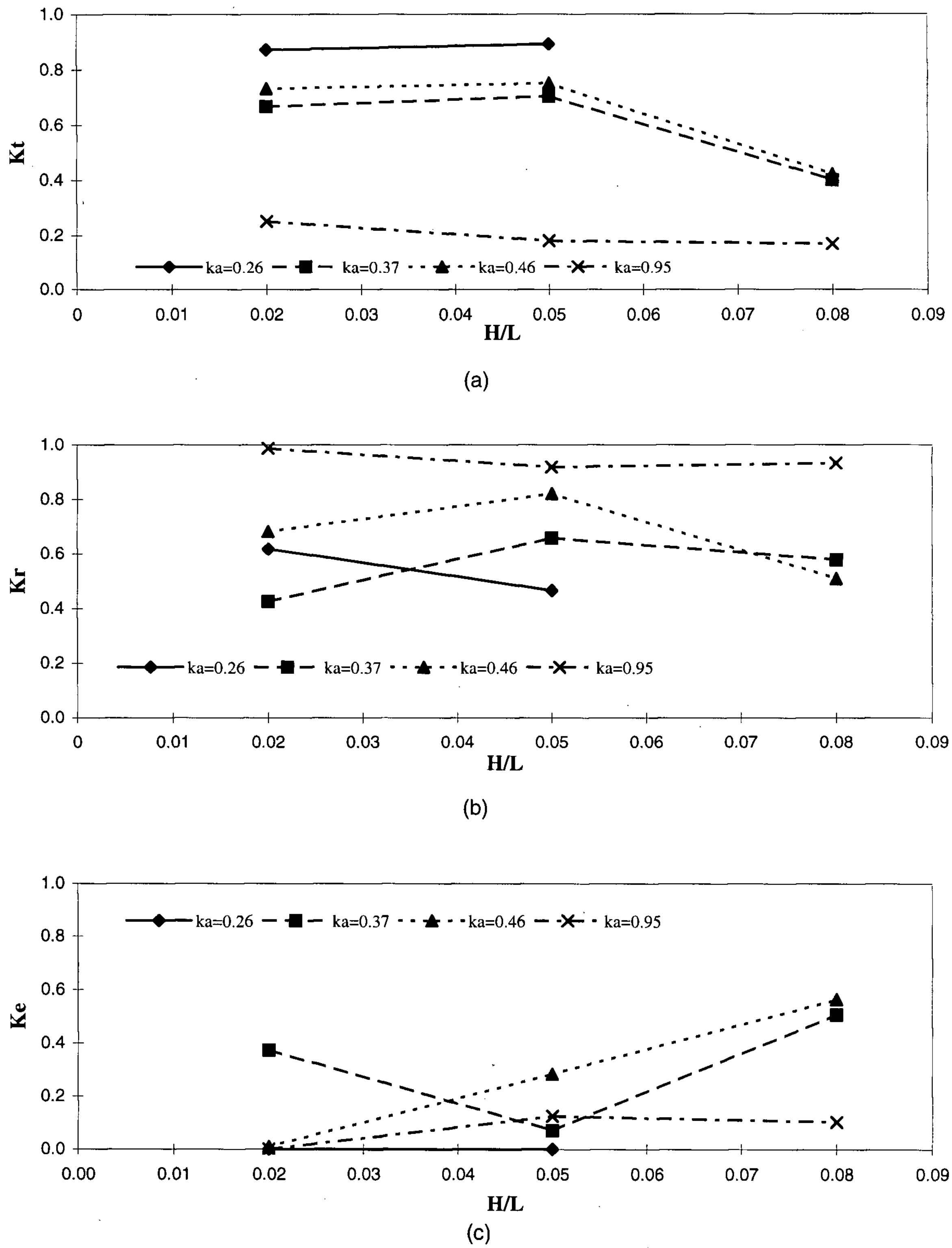

Figure 12. Hydrodynamic coefficients as a function of wave steepness with varying ka for the pile restrained case. (a) transmission coefficient, (b) reflection coefficient, (c) energy dissipation coefficient.

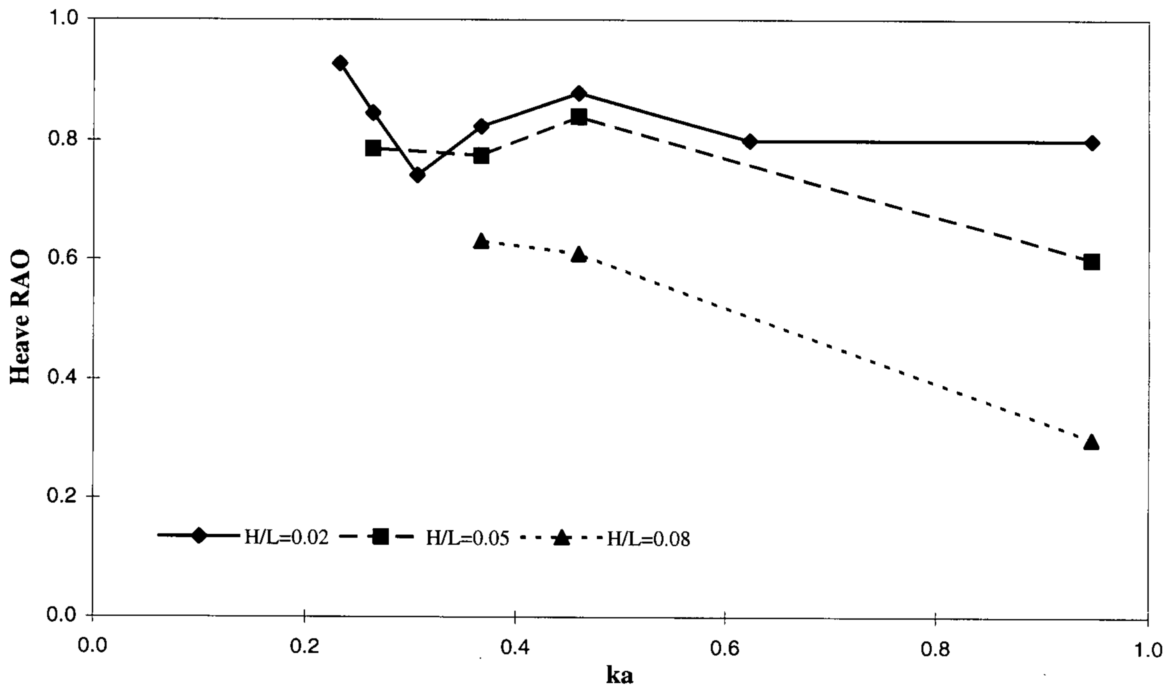

Figure 13. Heave RAO's as a function of ka for a varied steepnesses.

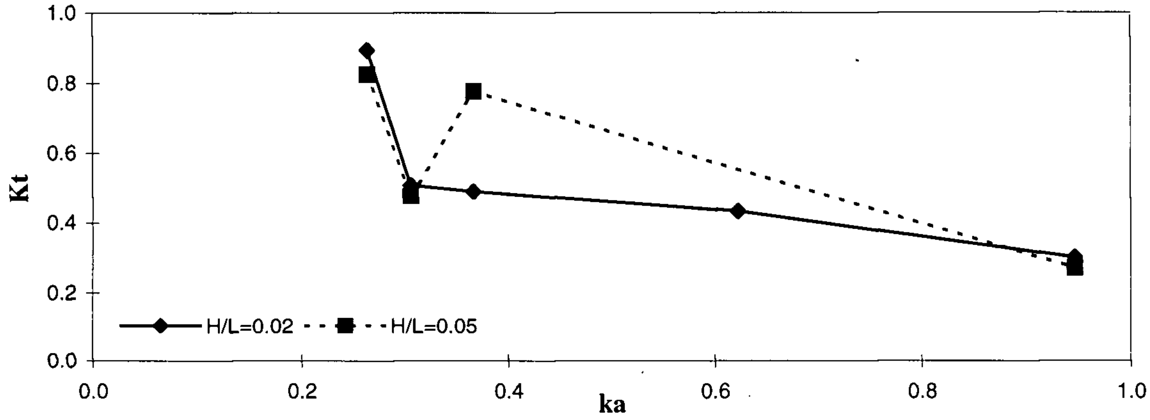

(a)

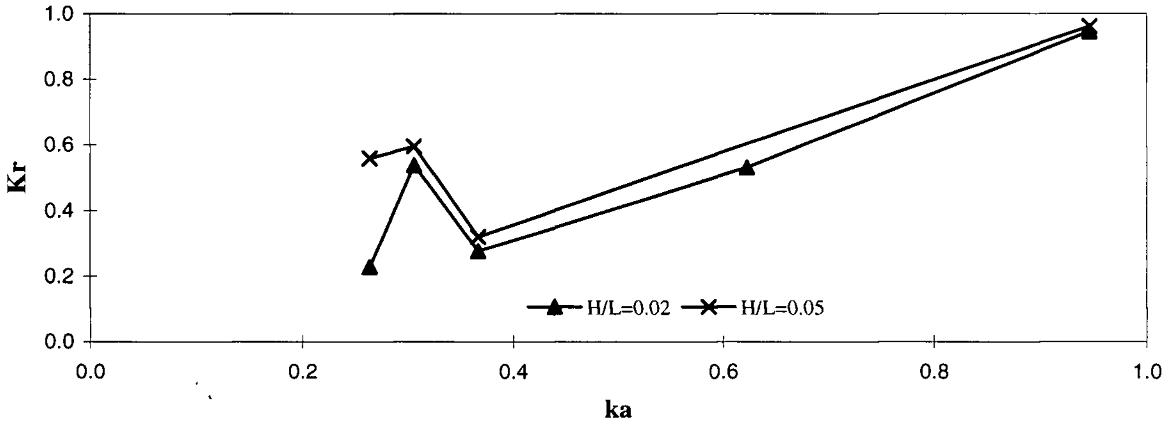

(b)

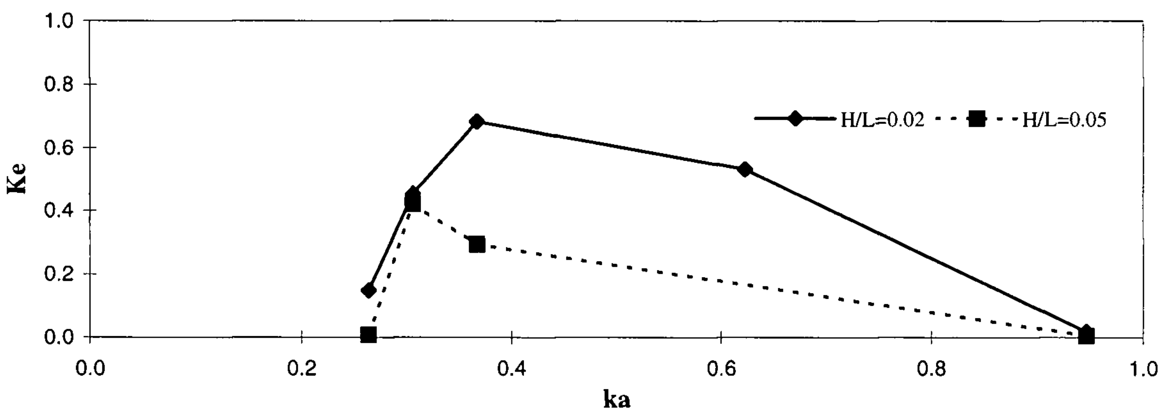

(c)

Figure 14. Hydrodynamic coefficients as a function of ka with varying wave steepness for the fixed case. (a) transmission coefficient, (b) reflection coefficient, (c) energy dissipation coefficient.

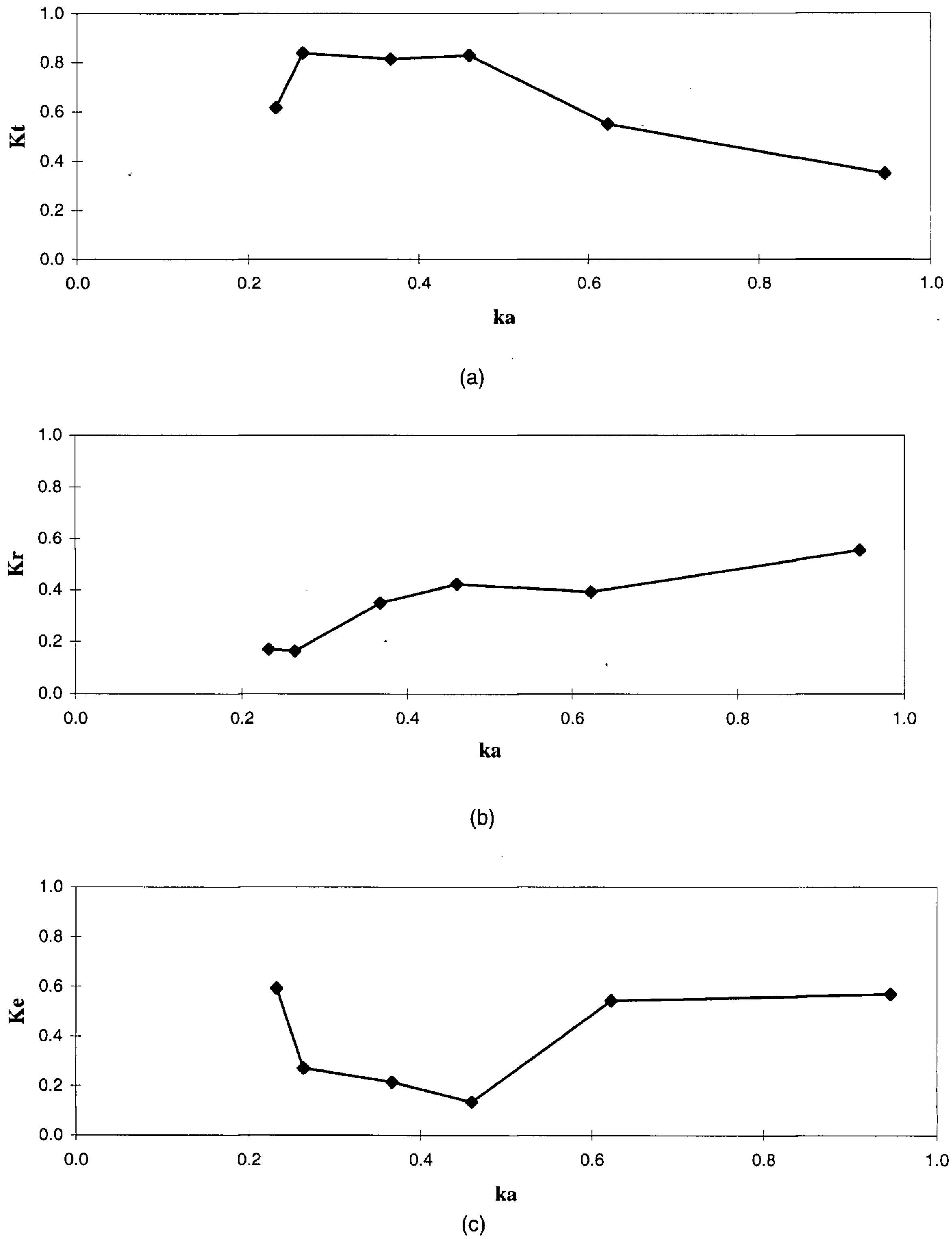

Figure 15. Hydrodynamic coefficients as a function of ka for the freely floating case with H/L = 0.02. (a) transmission coefficient, (b) reflection coefficient, (c) energy dissipation coefficient.

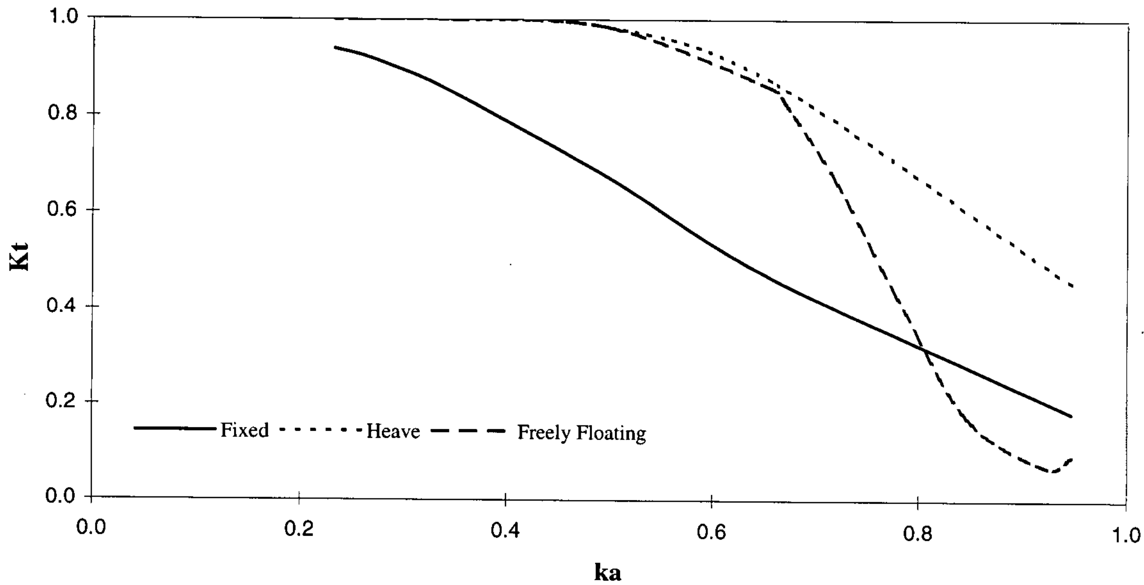

(a)

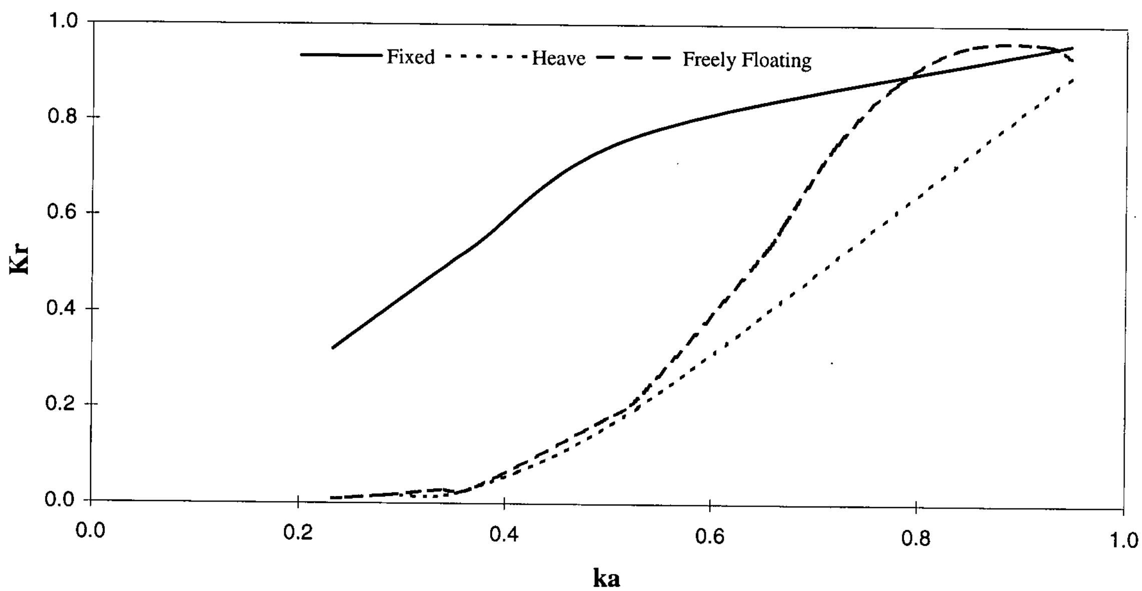

(b)

Figure 16. Numerically calculated hydrodynamic coefficients for the freely floating, fixed and pile restrained cases. (a) transmission coefficient, (b) reflection coefficient.

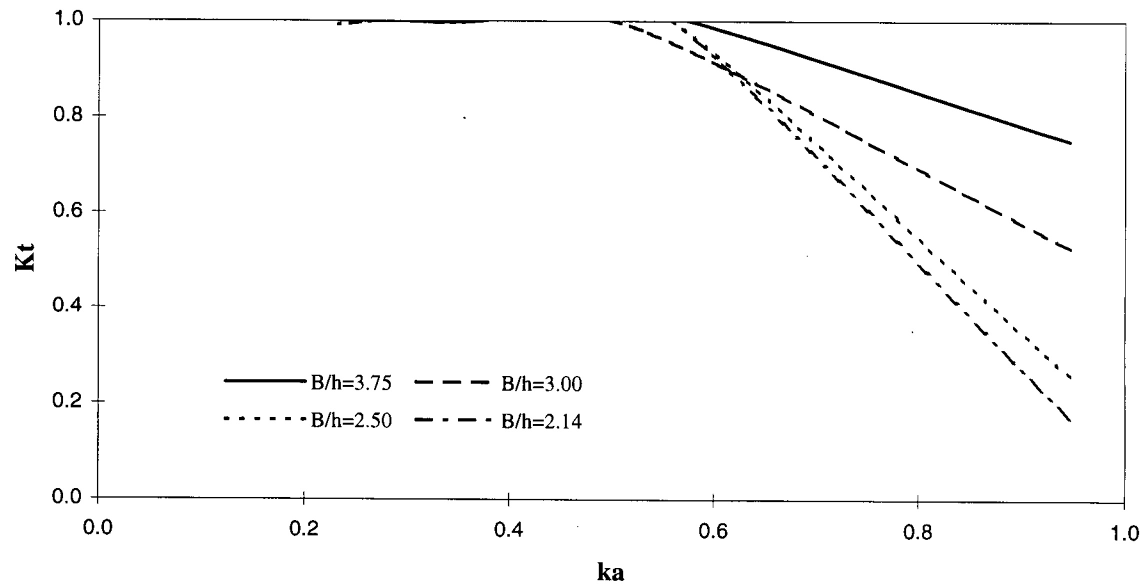

(a)

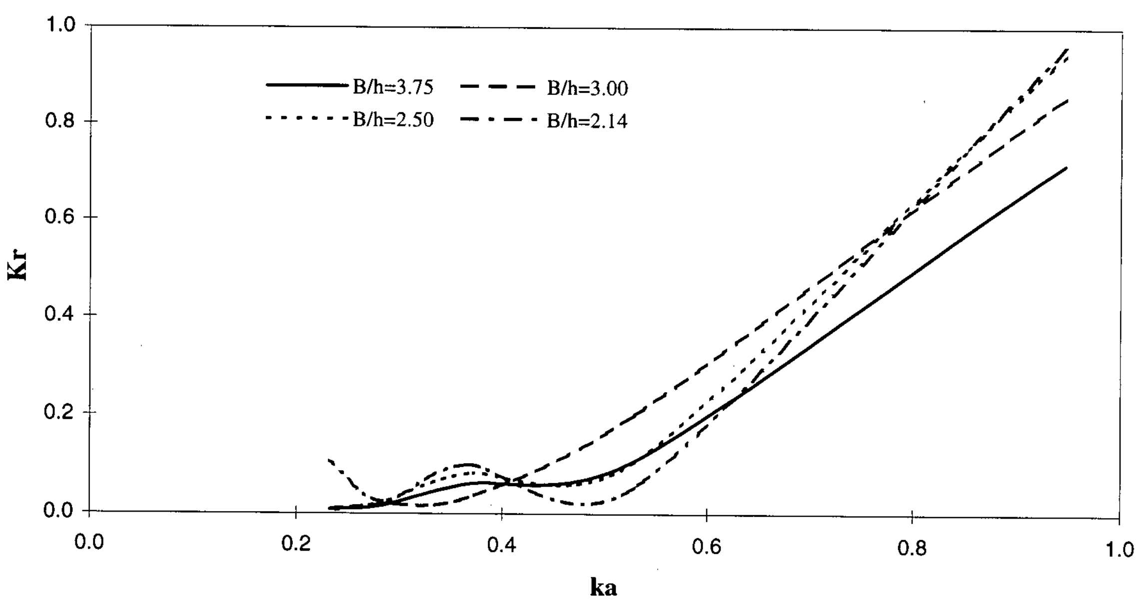

(b)

Figure 17. Influence of relative draft on numerically calculated hydrodynamic coefficients for the pile restrained case. (a) transmission coefficient, (b) reflection coefficient.

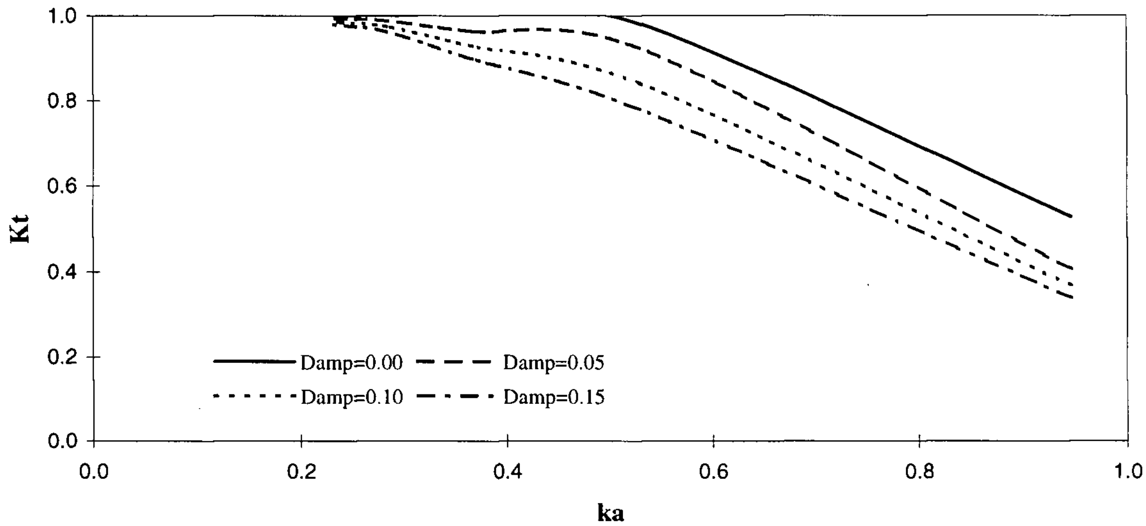

(a)

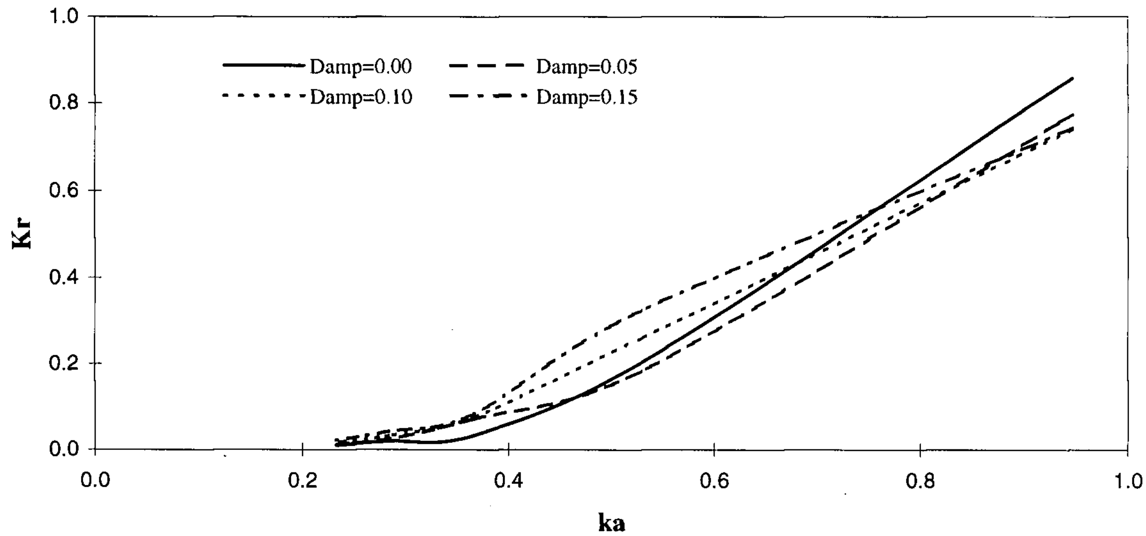

(b)

Figure 18. Influence of damping coefficient on numerically calculated hydrodynamic coefficients for the pile restrained case. (a) transmission coefficient, (b) reflection coefficient.

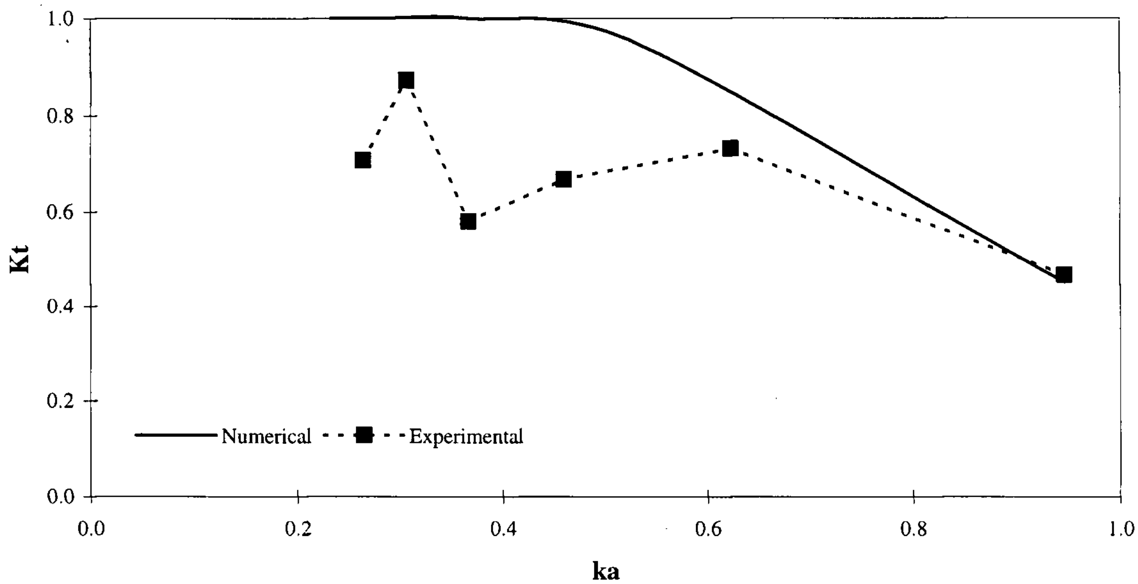

(a)

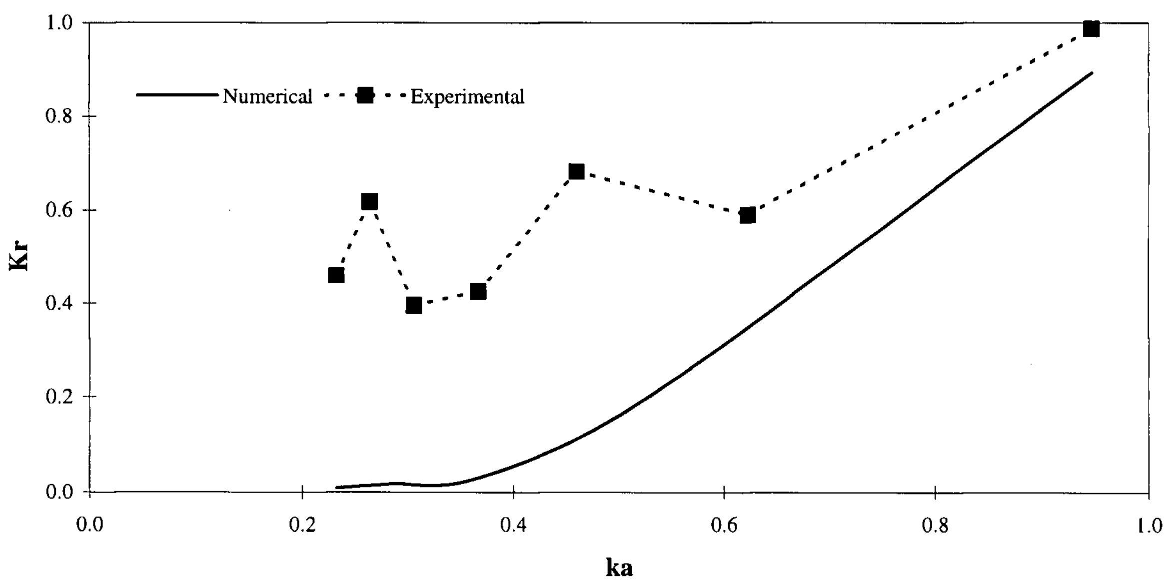

(b)

Figure 19. Comparison of numerical and experimental results of hydrodynamic coefficients for the pile restrained case (G = 4 cm, H/L = 0.02 in experiments). (a) transmission coefficient, (b) reflection coefficient.

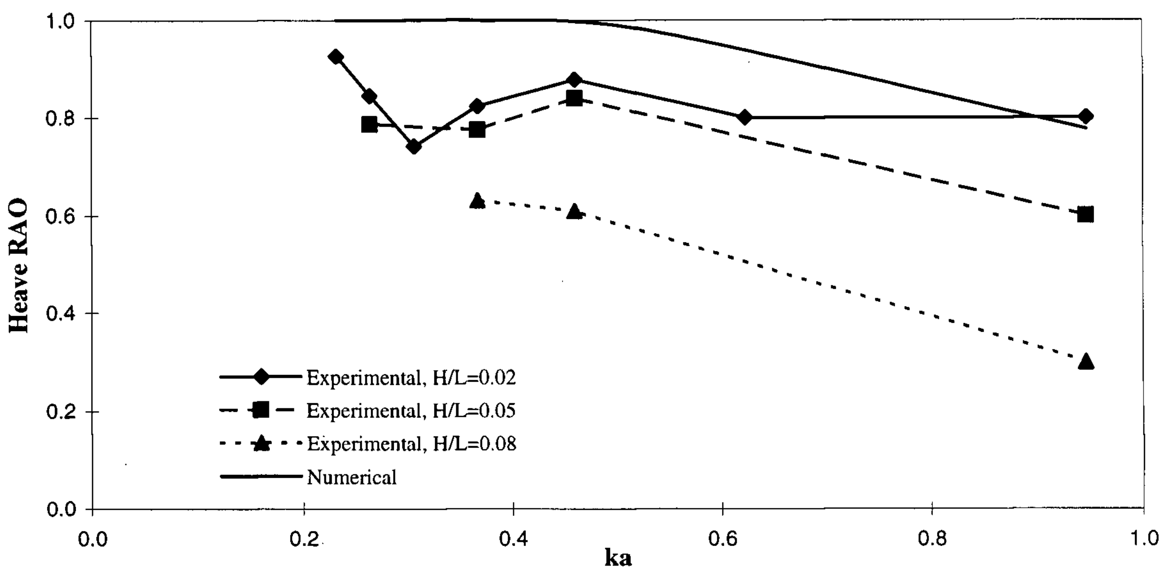

(a)

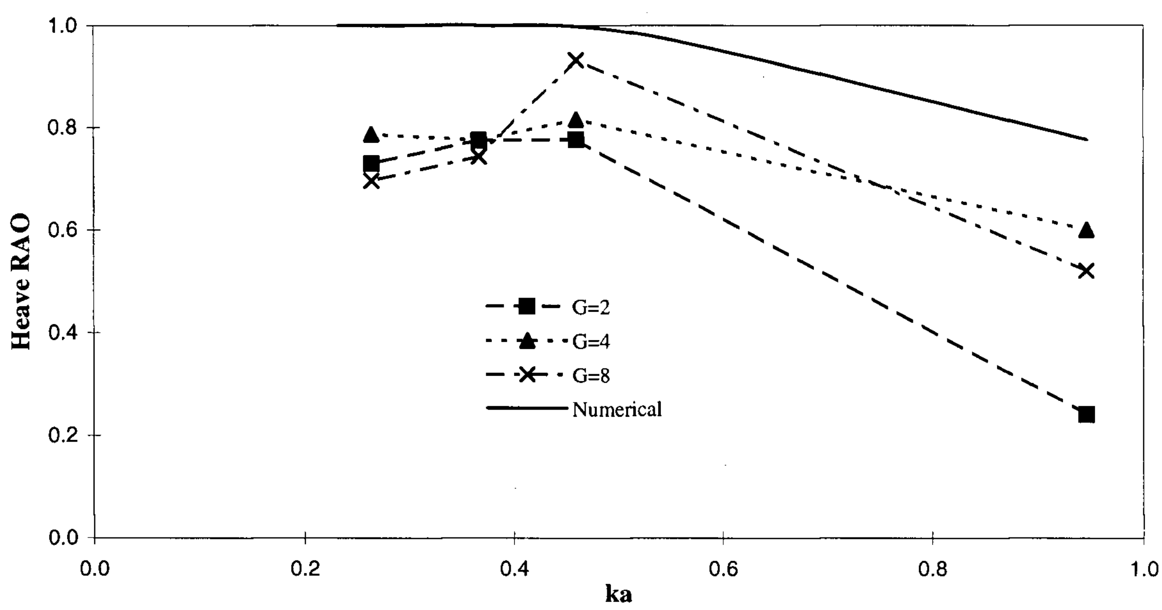

(b)

Figure 20. Comparison of numerical and experimental heave results for pile restrained case. (a) varying steepness, (b) varying gap (G in cm, H/L = 0.02).

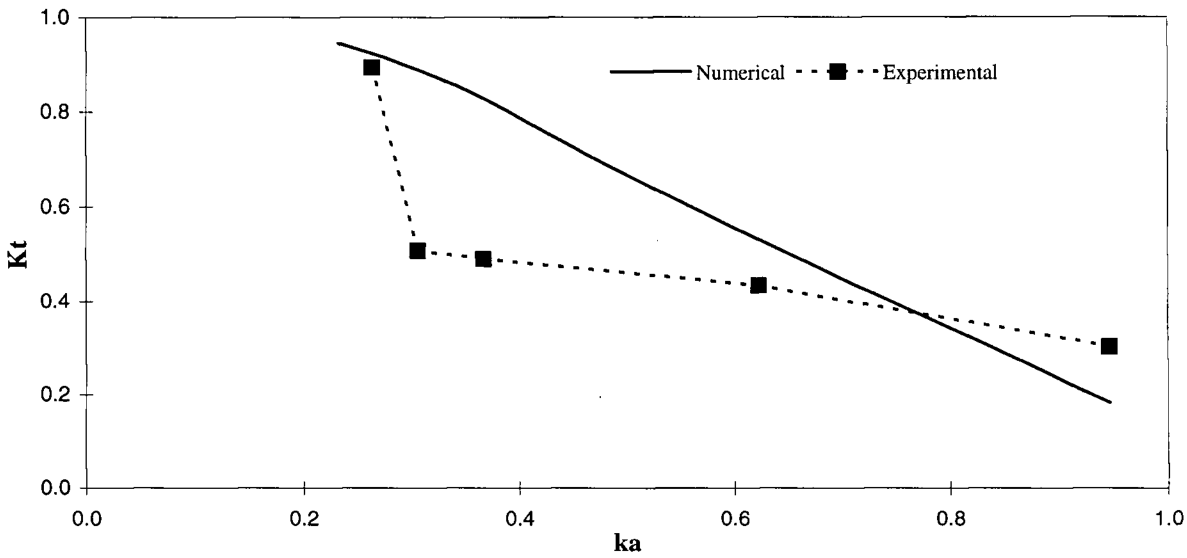

(a)

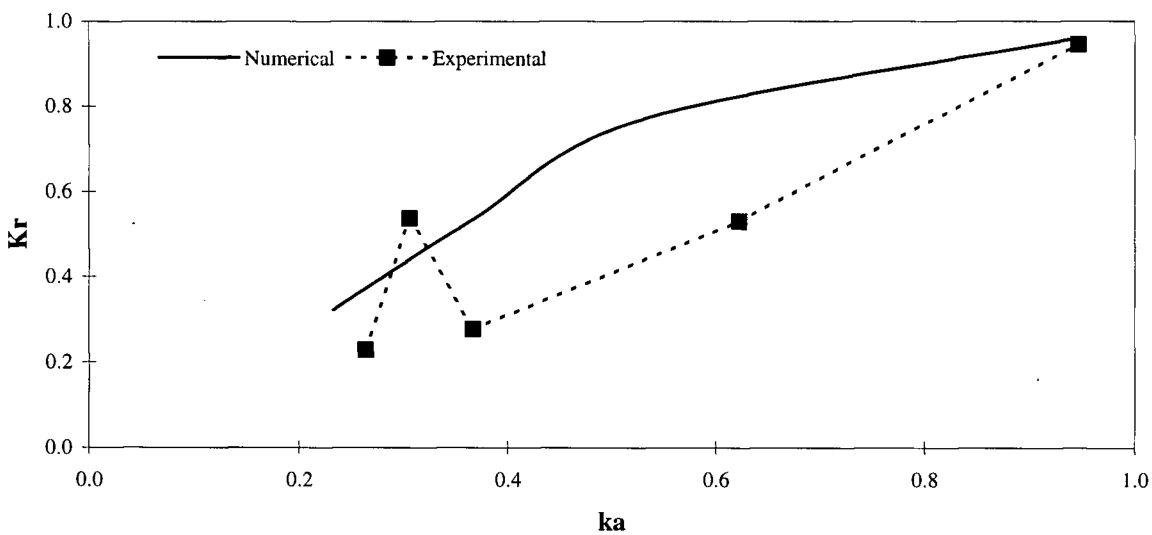

(b)

Figure 21. Comparison of numerical and experimental hydrodynamic coefficients for the fixed case. (a) transmission coefficient, (b) reflection coefficient.

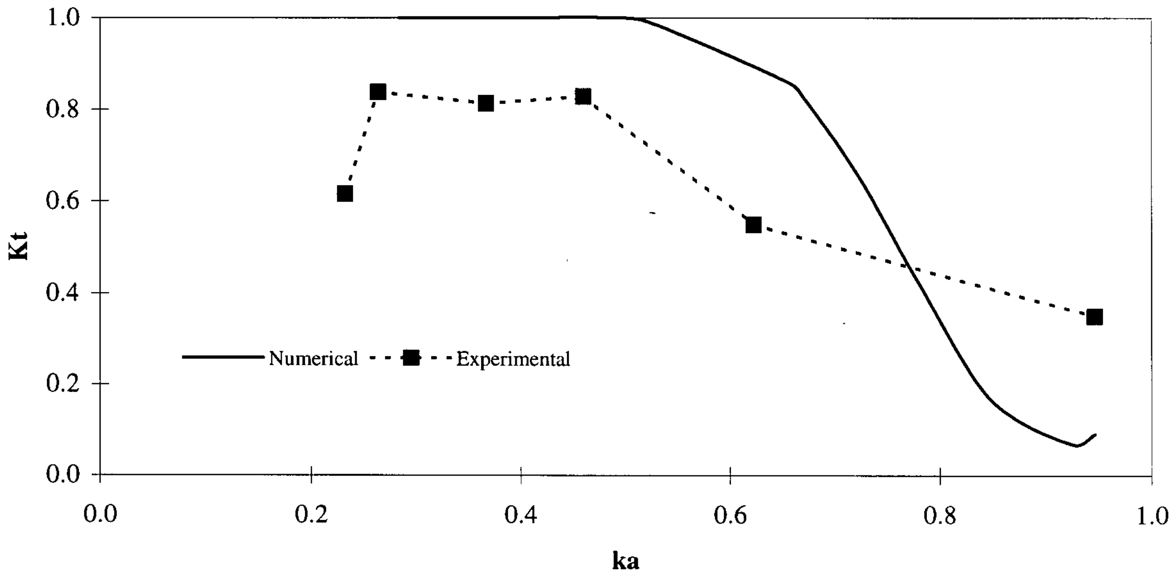

(a)

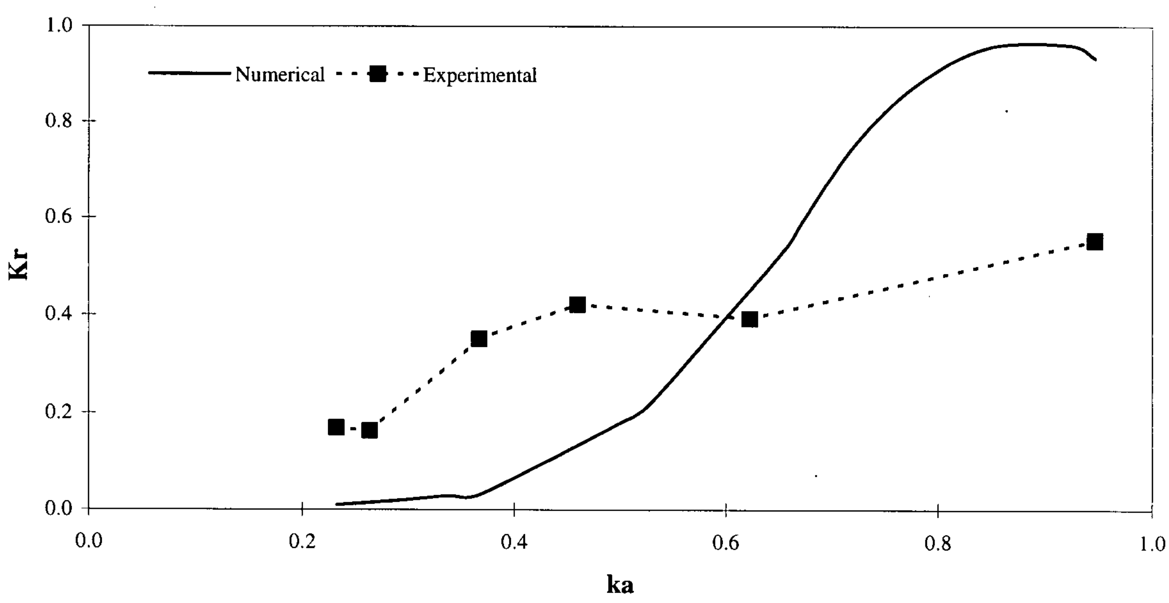

(b)

Figure 22. Comparison of numerical and experimental hydrodynamic coefficients for the freely floating case. (a) transmission coefficient, (b) reflection coefficient.